NASA-CR-168,206

NASA-CR-168206
19840002113

DEVELOPMENT OF ADVANCED INERT–GAS ION THRUSTERS

R. L. Poeschel

Hughes Research Laboratories
3011 Malibu Canyon Road
Malibu, CA 90265

June 1983

NAS3–22474
Final Report
16 June 1980 through 1 December 1982

NASA LEWIS RESEARCH CENTER
21000 Brookpark Road
Cleveland, OH 44135

```
    SELECT      E65                        SE107: INVALID SET NUMBER ARGUMENT
 30      1      1 RN/NASA-CR-168206
           DISPLAY 30/2/1
      84N10180*#   ISSUE 1   PAGE 29   CATEGORY 20   RPT#: NASA-CR-168206 NAS
      1.26:168206   CNT#: NAS3-22474   83/07/00  89 PAGES   UNCLASSIFIED
      DOCUMENT
UTTL: Development of advanced inert-gas ion thrusters   TLSP: Final Report
AUTH: A/POESCHEL, R. L.
CORP: Hughes Research Labs., Malibu, Calif.    AVAIL.NTIS   SAP: HC A05/MF A01
MAJS: /*ARGON/*ION PROPULSION/*ROCKET PROPELLANTS/*XENON
MINS: / CATHODES/ CUSPS/ MAGNETIC FIELDS
ABA:  S.L.
ABS:  Inert gas ion thruster technology offers the greatest potential for
      providing high specific impulse, low thrust, electric propulsion on large,
      Earth orbital spacecraft. The development of a thruster module that can be
      operated on xenon or argon propellant to produce 0.2 N of thrust at a
      specific impulse of 3000 sec with xenon propellant and at 6000 sec with
      argon propellant is described. The 30 cm diameter, laboratory model
      thruster is considered to be scalable to produce 0.5 N thrust. A high
      efficiency ring cusp discharge chamber was used to achieve an overall
      thruster efficiency of 77% with xenon propellant and 66% with argon
      propellant. Measurements were performed to identify ion production and
      loss processes and to define critical design criteria (at least on a
      preliminary basis).

ENTER:
```

TECHNICAL REPORT STANDARD TITLE PAGE

1. Report No. CR-168206	**2. Government Accession No.**	**3. Recipient's Catalog No.**

4. Title and Subtitle DEVELOPMENT OF ADVANCED INERT-GAS ION THRUSTERS	**5. Report Date** July, 1983
	6. Performing Organization Code
7 Author(s) R. L. Poeschel	**8. Performing Organization Report No.**
9. Performing Organization Name and Address Hughes Research Laboratories 3011 Malibu Canyon Road Malibu, CA 90365	**10. Work Unit No.**
	11. Contract or Grant No. NAS 3-22474
12. Sponsoring Agency Name and Address NASA Lewis Research Center 21000 Brookpark Road Cleveland, OH 44135	**13. Type of Report and Period Covered** Final Report
	14. Sponsoring Agency Code

15. Supplementary Notes

Project Manager: James Sovey, NASA Lewis Research Center,
Cleveland, Ohio

16. Abstract

Inert-gas ion thruster technology offers the greatest potential for providing high-specific-impulse, low-thrust, electric propulsion on large, earth-orbital spacecraft. This report describes the development of a thruster module that can be operated on xenon or argon propellant to produce 0.2 N of thrust at a specific impulse of 3000 sec with xenon propellant and at 6000 sec with argon propellant. The 30-cm-diameter, laboratory-model thruster is considered to be scalable to produce 0.5 N thrust. A high-efficiency ring-cusp discharge chamber was used to achieve an overall thruster efficiency of 77% with xenon propellant and 66% with argon propellant. Measurements were performed to identify ion production and loss processes and to define critical design criteria (at least on a preliminary basis).

17. Key Words (Selected by Author(s)) Electric propulsion Inert gas ion thruster Large communication satellites Solar power satellites	**18. Distribution Statement** Unclassified

19. Security Classif. (of this report) UNCLASSIFIED	**20. Security Classif. (of this page)** UNCLASSIFIED	**21. No. of Pages** 88	**22. Price***

*For sale by the Clearinghouse for Federal Scientific and Technical Information, Springfield, Virginia 22151.

N84-10180#

TABLE OF CONTENTS

LIST OF ILLUSTRATIONS

LIST OF ILLUSTRATIONS (Cont.)

LIST OF ILLUSTRATIONS (Cont.)

LIST OF TABLES

FOREWORD

The work described herein was performed primarily at Hughes Research Laboratories by the staff of the Plasma Physics Department. Several members of the department staff made major contributions during the conduct of the program and are recognized below:

J.R. Beattie - Program Manager and Principal Investigator 1980-1982

R.L. Poeschel - Program Manager and Principal Investigator 1982

S. Kami - Thruster Design and Fabrication

C.R. Dulgeroff - Thruster Tests

D.J. Hancock - Electronics Design

SUMMARY

The objective of this development program was to demonstrate feasibility for design and fabrication of an ion thruster to produce 0.5 N thrust operating with argon and/or xenon propellant. The approach used to demonstrate feasibility was to design, fabricate, and test a scaled model of the full-scale thruster design. Our initial analysis and design work paralleled the procedures formulated at Colorado State University for design of a multipole magnetic field ion thruster. Design drawings were prepared for the full-scale thruster and for a scaled-down laboratory model thruster (scaled to a 30-cm beam diameter)to permit operation in the NASA-Lewis Research Center test facility.

The initial results obtained in testing the scaled multipole thrust did not match the analytic predictions. The discharge ion production costs were higher than predicted and the propellant utilization was lower. There was evidence of plasma non-uniformity, even though the magnetic confinement cusps were well-matched in field strength. Furthermore, both the measured and predicted efficiencies of the multipole thruster were less than the thruster efficiencies obtained in the Lewis Research Center internal programs using high field-strength magnetic cusp geometry discharge chambers. In addition, the performance (efficiency) predicted analytically for the multipole discharge chamber thruster fell short of the program goals. At this point we adopted a ring-cusp discharge chamber design and proceeded to explore the benefits that it provides in comparison to the multipole discharge chamber.

The ring-cusp discharge chamber was found to be very efficient in terms of the power required for ion production. Minimum values of the discharge-chamber ion-production cost, $80 < \varepsilon_I < 90$ W/A, were quite reproducible and $\varepsilon_I = 100$ W/A was the nominal value required to produce useful propellant

efficiencies (about $\eta_m = 85\%$ for argon propellant, $\eta_P = 95\%$ for xenon propellant). Overall thruster efficiency was measured at $\eta_T = 66\%$ for argon and $\eta_T = 74\%$ for xenon. To determine the design criteria for the ring-cusp magnetic configuration that provides the observed efficient ion production, measurements of electron and ion currents were made at several isolated discharge-chamber electrodes and probes as functions of operating conditions and electrode bias. Analysis of these results infers that the control of electron loss by the high-field-strength magnet cusps results in a potential distribution that produces much stronger ion drift toward the ion extraction grid than occurs at the other discharge-chamber boundaries. The efficacy of the mechanism depends on the transparency of the extraction grid. For the measurements performed, no evidence was found to indicate the existence of any mechanism that completely prevents ion loss to any boundary of the discharge chamber.

The multipole discharge chamber, on the other hand, establishes a uniform electron loss to all anode surfaces by design, and thereby a uniform loss of ions to all discharge surfaces can be expected. In our initial multipole discharge chamber, a relatively large, distributed electron source was used to verify that stable operation of a thruster discharge chamber could be achieved with two hollow cathodes. While the two-cathode operation was verified, the abnormally large baffle area used to distribute electron emission was found to collect at least as many ions as reached the extraction grid. Therefore, in retrospect, poor ion production efficiency (per beam ampere) was to be expected.

In addition to demonstrating excellent thruster performance and documenting some of the critical ring-cusp thruster design features, several technologies useful for implementation in a 0.5 N thruster were verified. First, stable thruster operation was demonstrated using 30-cm-diameter ion extraction grids having a radius of curvature which would be appropriate for a 50-cm-diameter ion extraction assembly. In the course of fabricating these ion extraction grids for use under the program, several deficiencies in fabrication procedures were identified and solved. Second, it was shown that thermal control coatings can be applied to the discharge chamber to reduce the operating temperature (which may be required to operate the thruster at the maximum thrust density corresponding to space-charge limited ion extraction). Finally, a neutralizer using the same design as developed for mercury ion thrusters was shown to perform satisfactorily, although inefficiently, for operation of an inert-gas thruster.

SECTION 1

INTRODUCTION AND OVERVIEW

Work under this development program was a continuation of the work begun under NASA Contract NAS-321936 for "Analysis and Design of Ion Thrusters for Large Space Systems." Our initial approach under this previous study was to utilize the methodology formulated at Colorado State University[1,2] (under NASA-LeRC grants) to analyze and design a multipole-discharge-chamber type of ion thruster for producing a thrust of T = 0.5 N. Under the program reported here, this same methodology was used to scale the 0.5-N thruster to a size capable of being tested in the NASA-Lewis Research Center test facilities in a manner such that the critical design features could be evaluated.

A laboratory model of the scaled 30-cm-diameter thruster was fabricated and tested and the critical design features were verified. The performance (efficiency) of the scaled multipole thruster was inferior to that projected analytically and the prospects for exceeding the analytic projections to meet the program goals were considered poor. The discharge-chamber plasma model that has been used to describe (analytically) the ion production and loss processes in a multipole-magnetic-configuration discharge chamber postulates equal electron collection at all anodes and isotropic ion loss. Low values of ion production cost, ε_I, (power per beam ampere) cannot be projected (below about ε_I = 200 W/A) if ion production and loss occurs in accordance with this model.

At this point, our efforts were redirected to explore cusp-type discharge chambers, for which superior ion production costs are being observed (ε_I = 100 W/A). Cusp-type and multipole-type discharge chambers have the same generic magnetic field-shape that we have referred to as a "boundary" magnetic field because most of the discharge volume is essentially "field-free." Although there is no consistent terminology in the published literature, in this report we differentiate between multipole-type and cusp-type discharge chambers on the basis of whether electrons are collected at isolated anode surfaces that are "shielded" by the magnetic lines-of-force (multipole-type discharge) or whether electrons are collected in the magnetic cusps with anode potential pole-pieces (cusp-type discharge). Whereas multipole-type discharge chambers can be configured to operate with relatively low values of magnetic field without excessive electron loss, cusp-type discharge chambers require high field strength in the cusps (about 0.2 T or more) and consequently, electron loss is predominantly into the cusps along lines-of-force. Electron loss in cusp-type discharge chambers is considered to be dependent on configuration and less tractable to analysis than in multipole-type discharge chambers. This report emphasizes and concentrates on the results obtained with a cusp-type thruster discharge chamber; specifically, a ring-cusp configuration.

Technological advances were also realized in verifying novel design features developed for operation of larger diameter, higher thrust density thrusters. These demonstrations included operation of a discharge chamber with two or more cathodes, stable operation of ion extraction grids with 1.2 m radius of curvature (required to minimize thrust loss of a 50-cm diameter thruster), inert gas operation of "standard" hollow cathodes for both discharge chamber and neutralizer, pulsed operation of gas thrusters, and an anode-structure multipole discharge chamber design. These results are described in more detail in a separate section.

SECTION 2

RING-CUSP THRUSTER DEVELOPMENT

Extremely promising results have been reported earlier using cusp-type discharge chambers for reducing the ion-production cost, ε_I, in several types of gases, the most significant being the work of J. Sovey at NASA-Lewis Research Center.[3,4] The thruster configuration used for Hughes' investigation was based on the dimensions and magnetic field measurements obtained from Sovey's ring-cusp thruster discharge chamber. The techniques used to fabricate the Hughes ring-cusp thruster configuration and the experimental results obtained with this thruster are described in this section.

A. THRUSTER DESIGN CRITERIA AND SPECIFICATIONS

The Hughes ring-cusp thruster design was based on the magnetic configuration specifications obtained from NASA-LeRC in the form of equi-magnitude contours of magnetic field and approximate magnet locations, as shown in Figure 1 (dashed curves). The thruster discharge-chamber diameter was determined by the inside diameter of the 30-cm thruster ion-extraction-assembly mountings already in use (and also by the standard steel-pipe sizes available). The discharge chamber is constructed quite simply, using a welded steel pipe as the side-wall (31.8-cm inside diameter) and a flat steel plate as the upstream boundary. A true cylindrical shape was ensured by constraining the pipe within two heavy steel rings that fit tightly over the outside diameter of the tube; one of these rings also serves as the mounting for the ion-extraction assembly. The steel cylinder was "grit-blasted" inside and out to provide better thermal radiation properties. The magnets that form the "ring-cusp" are rectangular in shape (1.9-cm long by 1.3-cm wide by 0.5-cm high, and magnetized along the short dimension) and are installed in rings around the interior surface of the discharge

12641—4

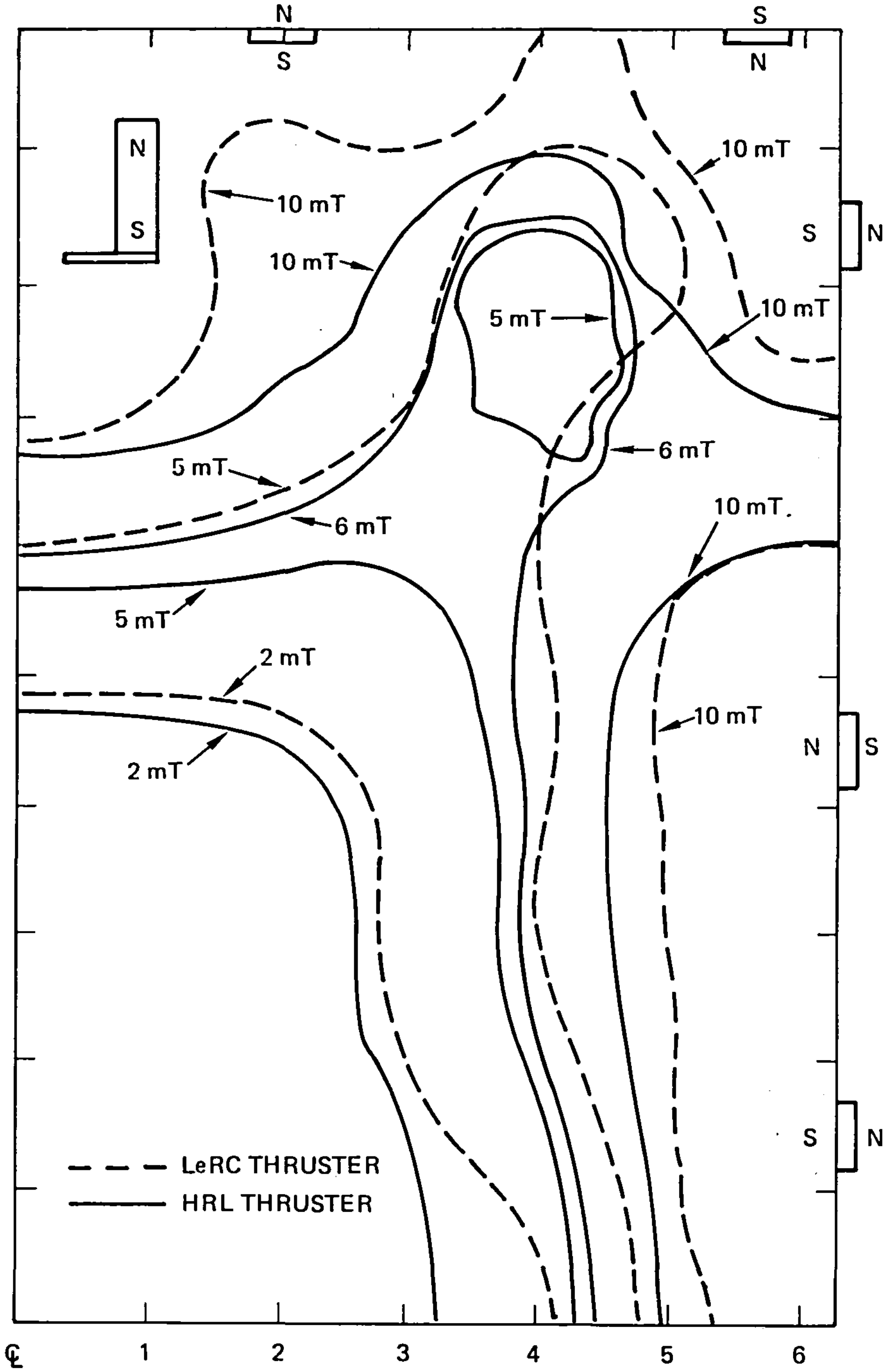

Figure 1. Equimagnitude magnetic field contours (equal values of $B_z^2 + B_r^2$) measured in the NASA-LeRC and HRL ring-cusp thrusters.

chamber. The magnets are held in place only by the magnetic attraction to the steel discharge-chamber walls, as shown in cross-section in Figure 1. The position of the rings was adjusted to obtain the equimagnitude contours shown as solid curves. Equimagnitude contours were obtained by measuring the axial (B_z) and radial (B_r) components of the magnetic field and computing the square root of the sum of the squares ($\sqrt{B_z^2 + B_r^2}$) for each measurement point. These measured values are cross-plotted as functions of radial or axial position to permit location of equimagnitude points. Measurements on a grid of 1.27-cm squares provides a sufficient number of points to obtain smooth contours.

To determine the location of the cathode in the cathode magnet, the axial component of the magnetic field was measured to obtain a plot like the one shown as Figure 2. The optimum cathode location is considered to be just downstream of the maximum.[5] The

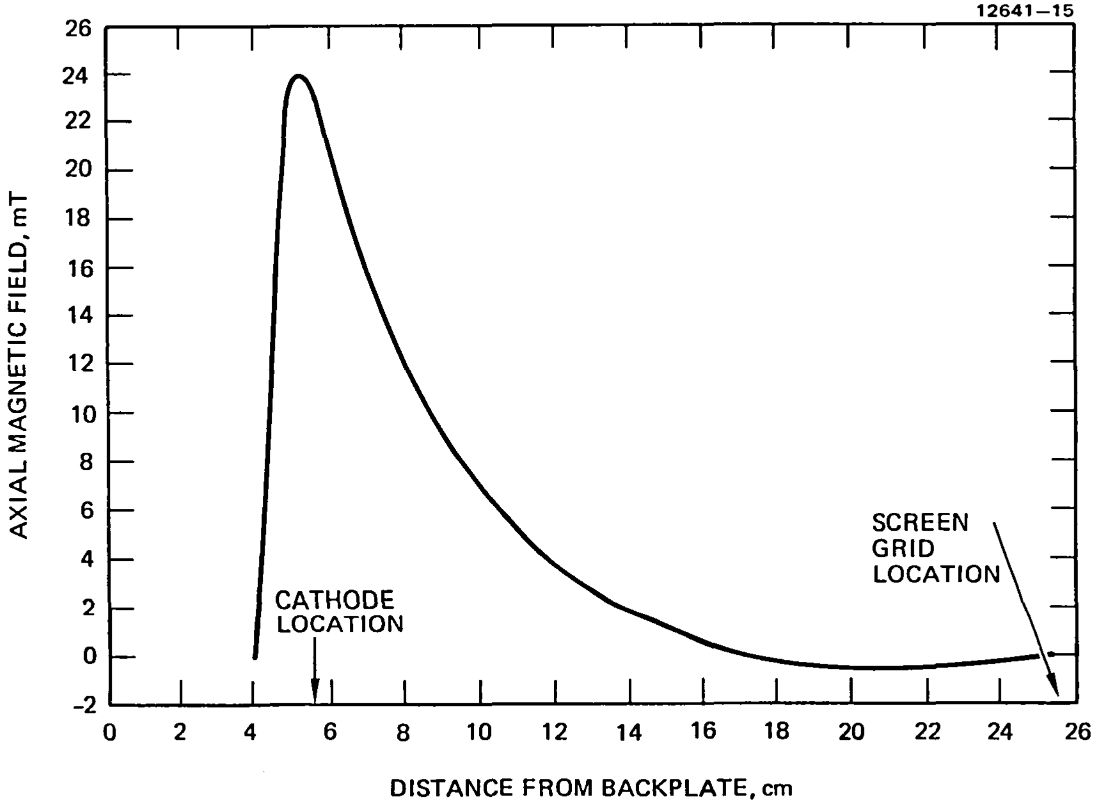

Figure 2. Cathode location with respect to the axial magnetic field strength in the 30-cm diameter ring cusp thruster.

cathode magnet was constructed by strapping cylindrical alnico magnets (0.64-cm diameter by 2.5-cm long) around a stainless steel pipe. The diameter of the pipe (and the number of magnets) was varied until the maximum value of the curve shown in Figure 2 was more than 200 gauss. Addition of an iron washer as a pole-piece on the end of these magnets aided in increasing this peak value.

To complete the documentation of the magnetic field, the lines-of-force were mapped using powdered iron. By lining the discharge chamber with polyethylene film, powdered iron was "dusted" onto white cardboard coated with clear lacquer that had been allowed to dry until tacky. In this manner, the powdered iron produces a pattern that is aligned with the magnetic lines of force, even though the magnetic force exerted on the powdered iron attracts a large fraction of the iron to the magnets and pole-pieces. When the lacquer dried completely, the cardboard was removed and the pattern was traced, distributing the lines of force at about equal spacing to produce a pattern like that shown in Figure 3. The data shown in Figures 1 through 3 are considered to completely specify the magnetic field for the 30-cm ring-cusp thruster.

The thruster discharge chamber shown in Figure 3 is operated so that all surfaces are at anode potential except the cathode, the cathode magnet, and the screen electrode (which are all operated at cathode potential). Figure 4 shows a photograph of the interior of the discharge chamber with the ion-extraction assembly removed. One of the rings of magnets is clearly visible; however, the other four are covered by thin shields that permit the electron current collected at each cusp to be monitored. The magnet cover construction is shown as Figure 5. These magnet covers reduce the field strength at the surface of the cusp by about 20-30 mT; however, little difference was noted in the discharge operation (without extraction of an ion beam). The magnet covers also serve to shield the magnets from the discharge thermal input and permit operation at higher discharge powers for longer time periods. Thermocouples were attached to the inner and outer surfaces

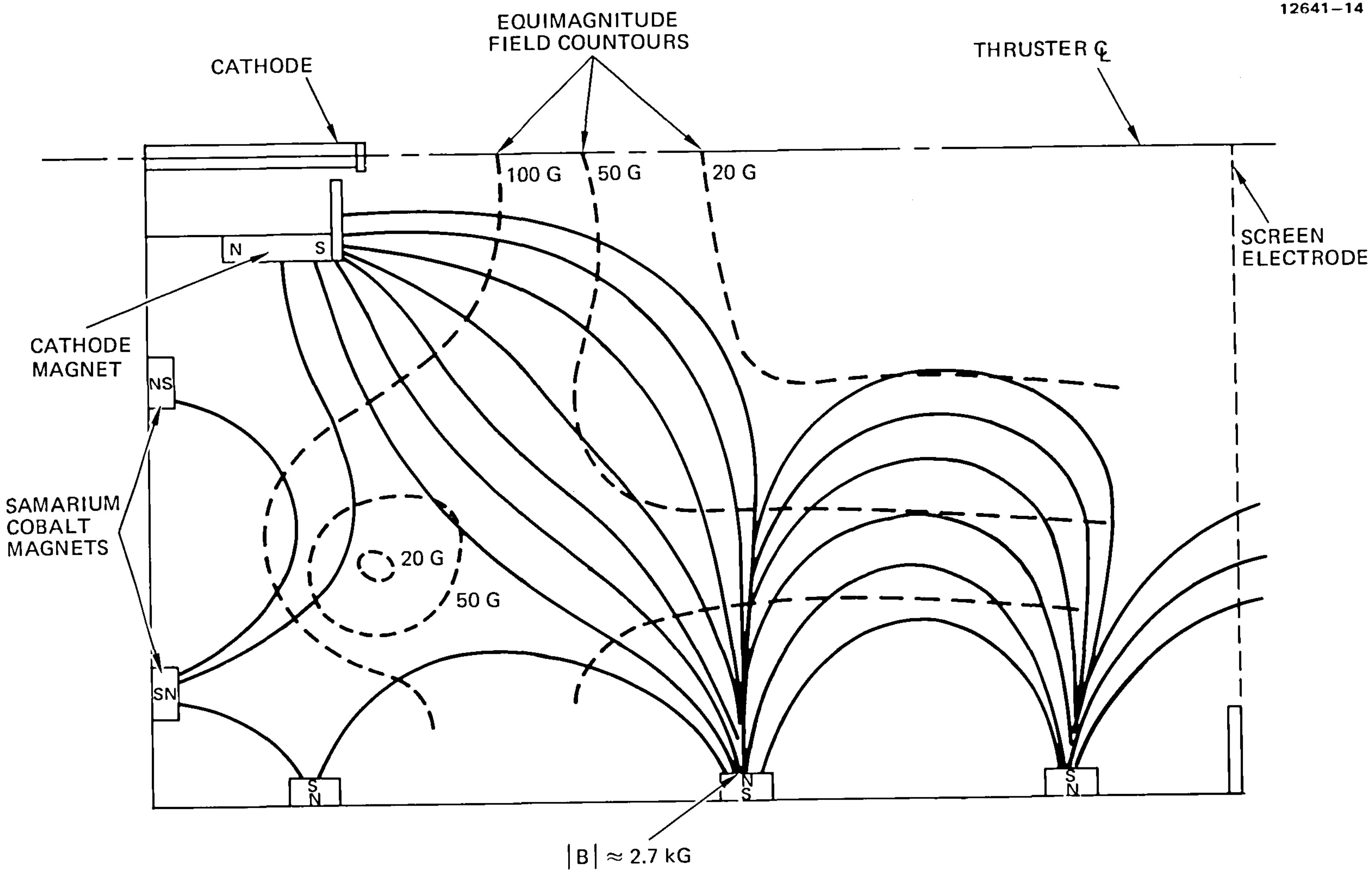

Figure 3. Magnetic field lines-of-force and equimagnitude contours for the 30-cm ring-cusp thruster.

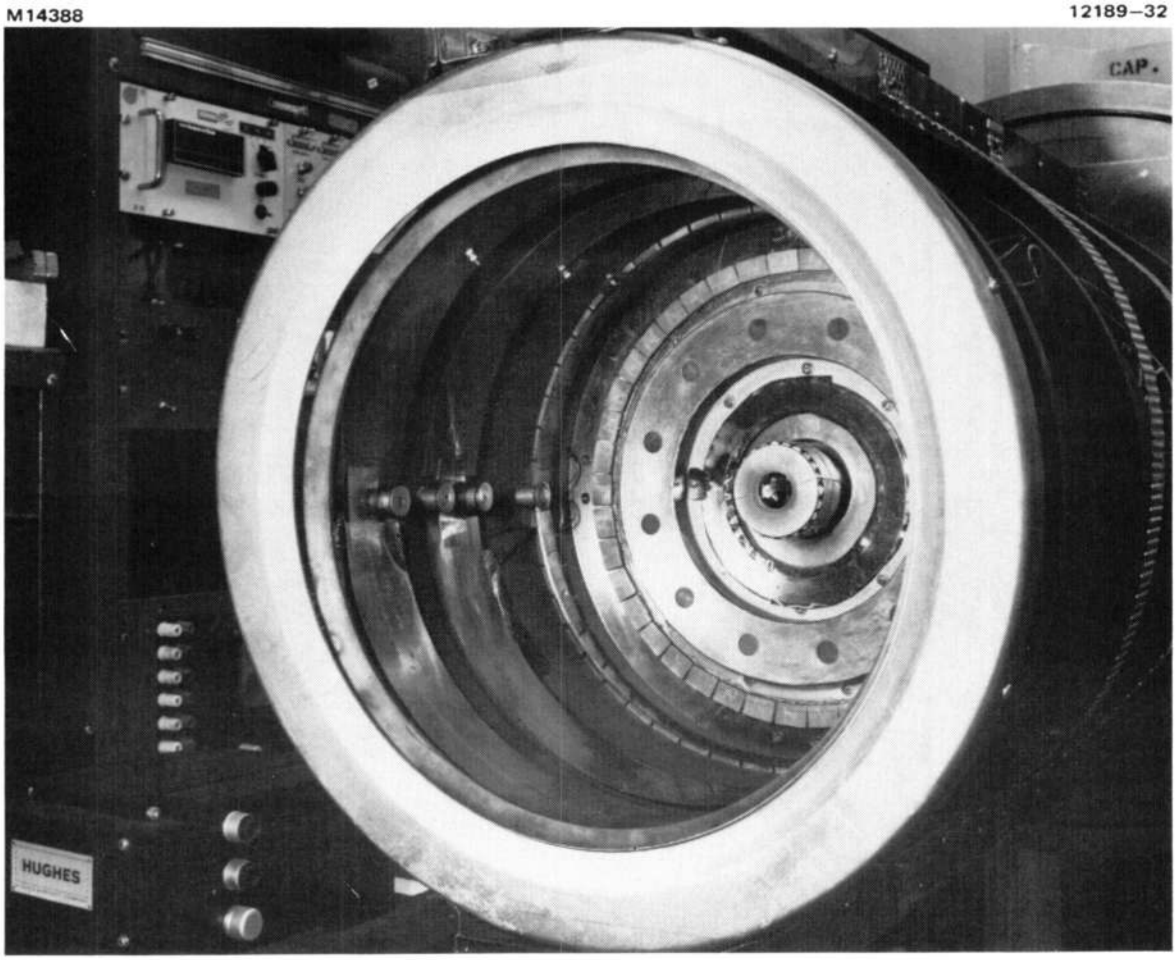

Figure 4. Hughes laboratory-model 30-cm argon ring-cusp discharge chamber.

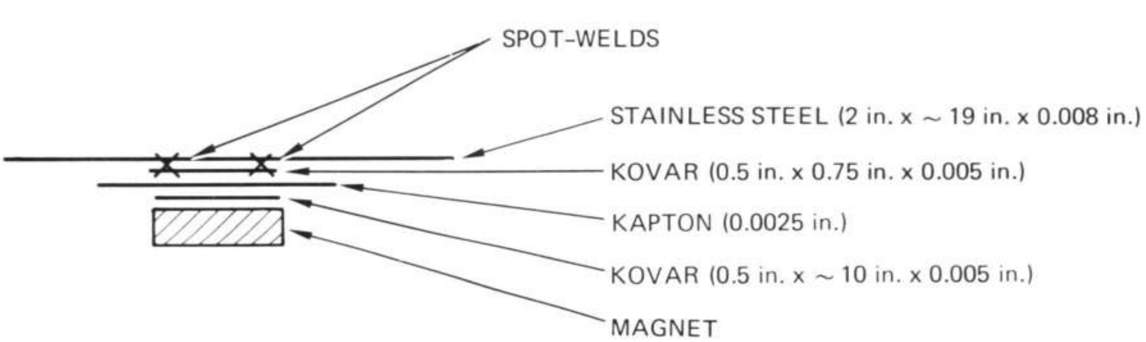

Figure 5. Final iteration on magnet covers for sidewall ring-cusp magnets. All cover pieces have expansion clearance to prevent buckling.

of the magnets to monitor temperatures so that the upper limit of reversible, thermal demagnetization was not exceeded.

Also visible in Figure 4 are four wall probes used to monitor ion currents to the side wall. Figure 6 shows a cross-section of the construction details of these probes. The location of these

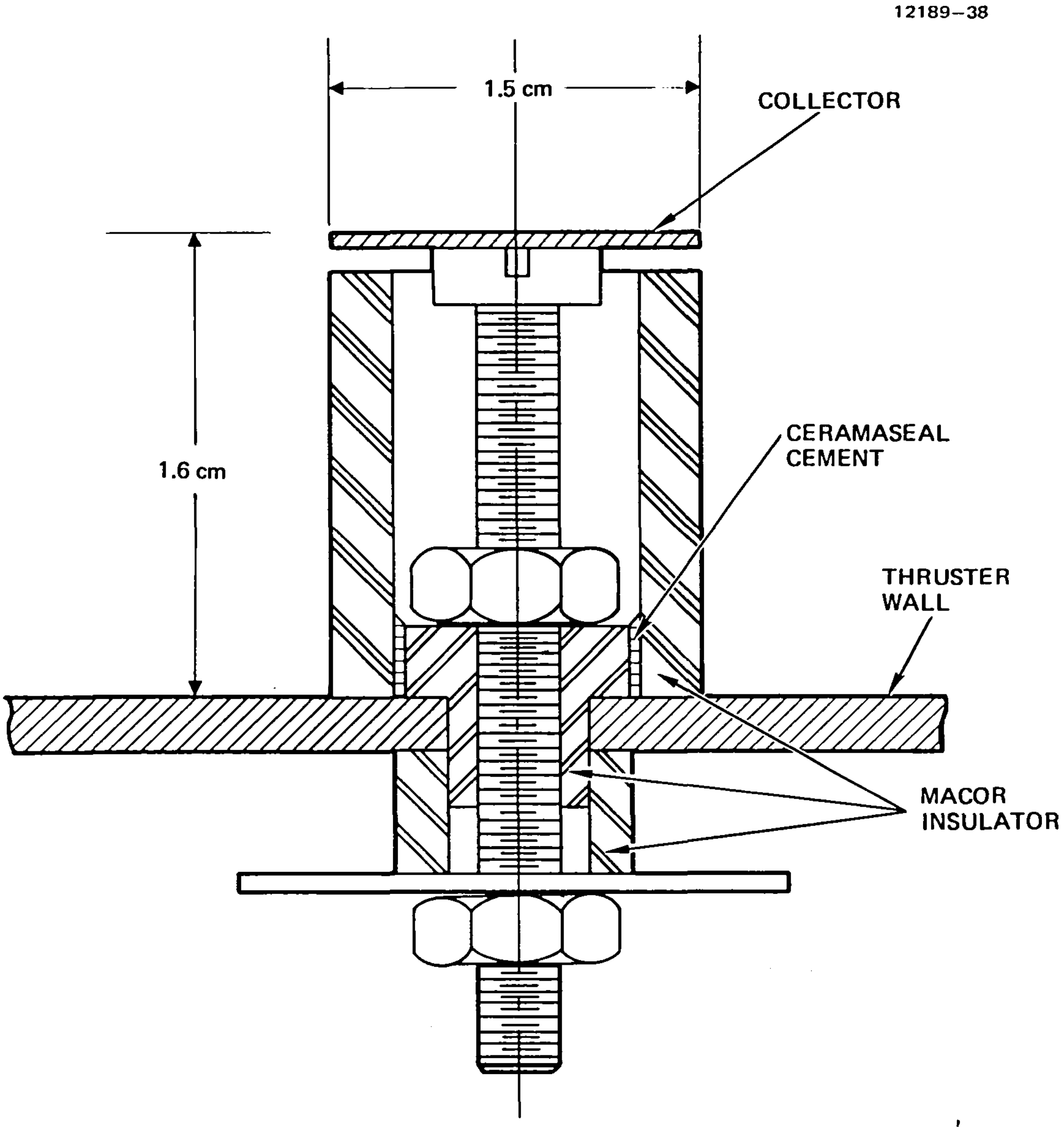

Figure 6. Cross-section showing construction detail of the wall probe.

probes in relation to the magnet cusps, the magnetic lines-of-force, and other discharge chamber elements is shown in Figure 7. Figure 7 also shows the location of a stationary Langmuir probe that was installed for some of the thruster measurements.

Three different sets of ion-extraction assemblies were used in testing the ring-cusp thruster. These assemblies had grid specifications, as shown in Table 1. Grid sets A and B were fabricated under the contract and were used for the tests conducted at Hughes Research Laboratories and at the NASA-Lewis Research Center. Grid set C was furnished by NASA for tests at Lewis Research Center when problems occurred with grid sets A and B.

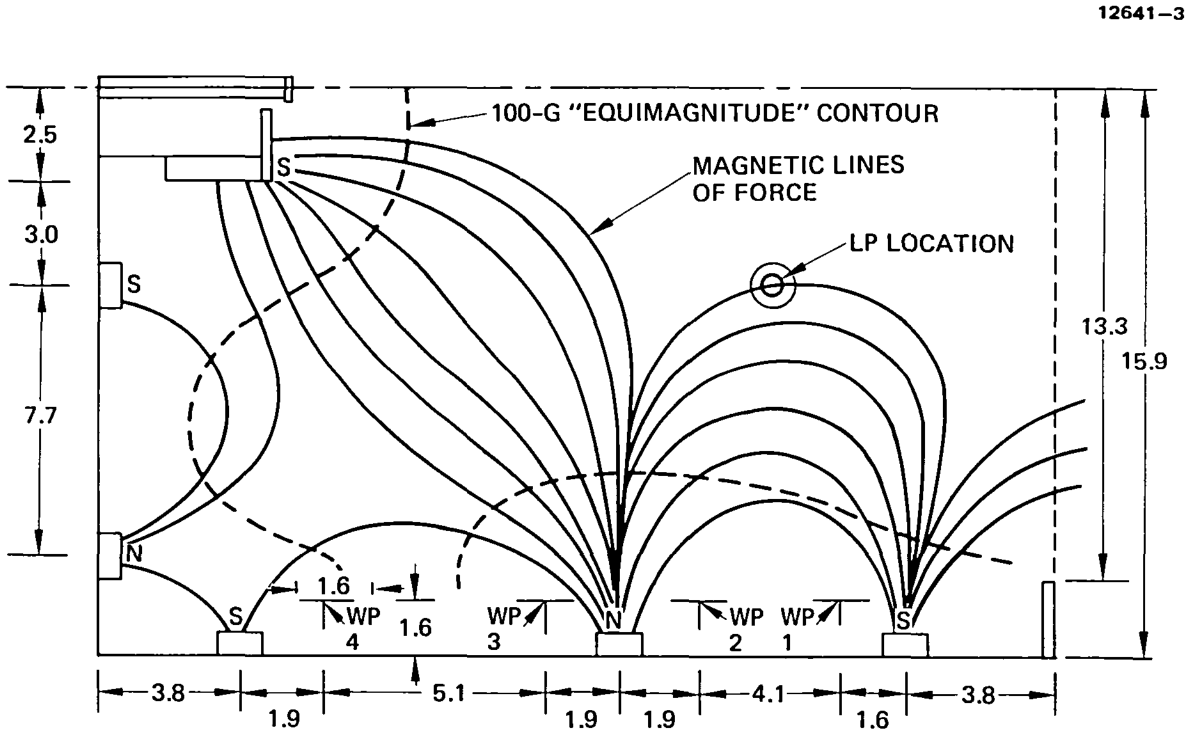

Figure 7. Ring-cusp discharge chamber showing the magnetic lines of force (determined by using iron filings), wall probes, and the 100-G "equimagnitude" contour (all dimensions in cm).

Table 1. Grid Specifications for the Ion Extraction Assemblies Used for Evaluation of the Ring-Cusp Thruster

Design Parameter	Ion Extraction Assembly		
	A 2-Grid Standard Dish	B 3-Grid Shallow Dish	C 2-Grid Standard Dish
Screen Grid*			
Hole Diameter, cm (in.)	0.190(0.075)	0.190(0.075)	0.190(0.075)
Center-to-Center Spacing, cm (in.)	0.2202(0.08669)	0.22058(0.08684)	(Hexagonal)
(% Reduction in Hole Pattern)	(0.35)	(0.18)	Not Specified
Open Area Fraction	0.68	0.68	0.75
Accel Grid*			
Hole Diameter, cm (in.)	0.1143(0.045)	0.1143(0.045)	0.1143(0.045)
Center-to-Center Spacing, cm (in.)	0.220 (0.087)	0.22098(0.98700)	0.220(0.087)
Open Area Fraction	0.24	0.24	0.27
Decel Grid*			
Hole Diameter, cm (in.)	N/A	0.1524(0.060)	N/A
Center-to-Center Spacing, cm (in.)	N/A	0.22087(0.08696)	N/A
(% Reduction in Hole Pattern)	N/A	(0.04)	N/A
Open Area Fraction	N/A		N/A
Screen – Accel Spacing, cm (in.)	0.066(0.026)	0.071(0.028)	0.066(0.026)
Accel – Decel Spacing, cm (in.)	N/A	0.071(0.028)	N/A
Minimum Total Voltage at 2 A Beam Current (Hg Ions), V	1320	1435	1320
Dish Depth, cm (in.)	2.18(0.86)	0.899(0.354)	2.18(0.86)
(Radius of Curvature, M)	(0.50)	(1.25)	(0.50)

*All grid thicknesses 0.038 cm (0.015 in.).

To facilitate the description of the thruster and discharge chamber performance characteristics, a list of symbols and definitions has been prepared and is provided in Table 2. A diagram showing the measurement location of various electrode currents and voltages is presented as Figure 8. The data described in this report have been processed to conform to the definitions and descriptions provided in Table 2 and Figures 4 and 5, even though the data may have been reported in the monthly reports in another format. Some relationships between the quantities defined in Table 2 are as follows:

$$J_I = J_E + J_{CM} + J_{SG} \tag{1}$$

$$P_D = V_D J_I \tag{2}$$

$$\varepsilon_I = \frac{P_D}{J_B} \tag{3}$$

$$J_D = J_B + J_I \tag{4}$$

$$P_B = V_B J_B \tag{5}$$

$$P_{TOT} = P_B + P_D + V_g J_B + V_{NK} J_{NK} \tag{6}$$

$$\eta_e = \frac{P_B}{P_{TOT}} \tag{7}$$

$$\eta_T = \gamma^2 \eta_e \eta_M \tag{8}$$

$$I_{SP} = \frac{\gamma \eta_m}{g_o} \left(\frac{2eV_B}{m_i}\right)^{1/2} \tag{9}$$

Table 2. Definitions of Symbols

V_B	Beam Voltage, V
J_B	Beam Current, A
V_{ac}	Accelerator Electrode Voltage, V
J_{ac}	Accelerator Electrode Current, A
J_{P1} to J_{P4}	Wall Probe Current
V_{WP}	Wall Probe Bias Voltage
WP	Wall Probe
J_{CM}	Current collected on the cathode magnet subassembly
J_E	Cathode Emission Current
J_I	Current required for ionization processes
J_{SG}	Current collected by the screen grid
J_{A1} to J_{A4}	Current collected on ring cusp anode electrodes
J_{AS}	Current collected on the anode shell
V_D	Discharge Voltage
J_D	Discharge Current
V_g	Neutralizer Coupling Voltage (voltage from neutralizer common to ground)
V_{NK}	Neutralizer Keeper Voltage
J_{NK}	Neutralizer Keeper Current
LP	Langmuir Probe
V_{LP}	Langmuir Probe Voltage
J_{LP}	Langmuir Probe Current
P_D	Discharge Power
P_B	Beam Power
P_{TOT}	Total Input Power
ε_I	Ion Production Cost, W/A
η_e	Electrical Efficiency
η_{MD}	Discharge Propellant Utilization Efficiency
η_M	Thruster Propellant Utilization Efficiency
η_T	Thruster Efficiency
γ	Thrust Loss Correction Factor
I_{SP}	Specific Impulse
F	Thrust

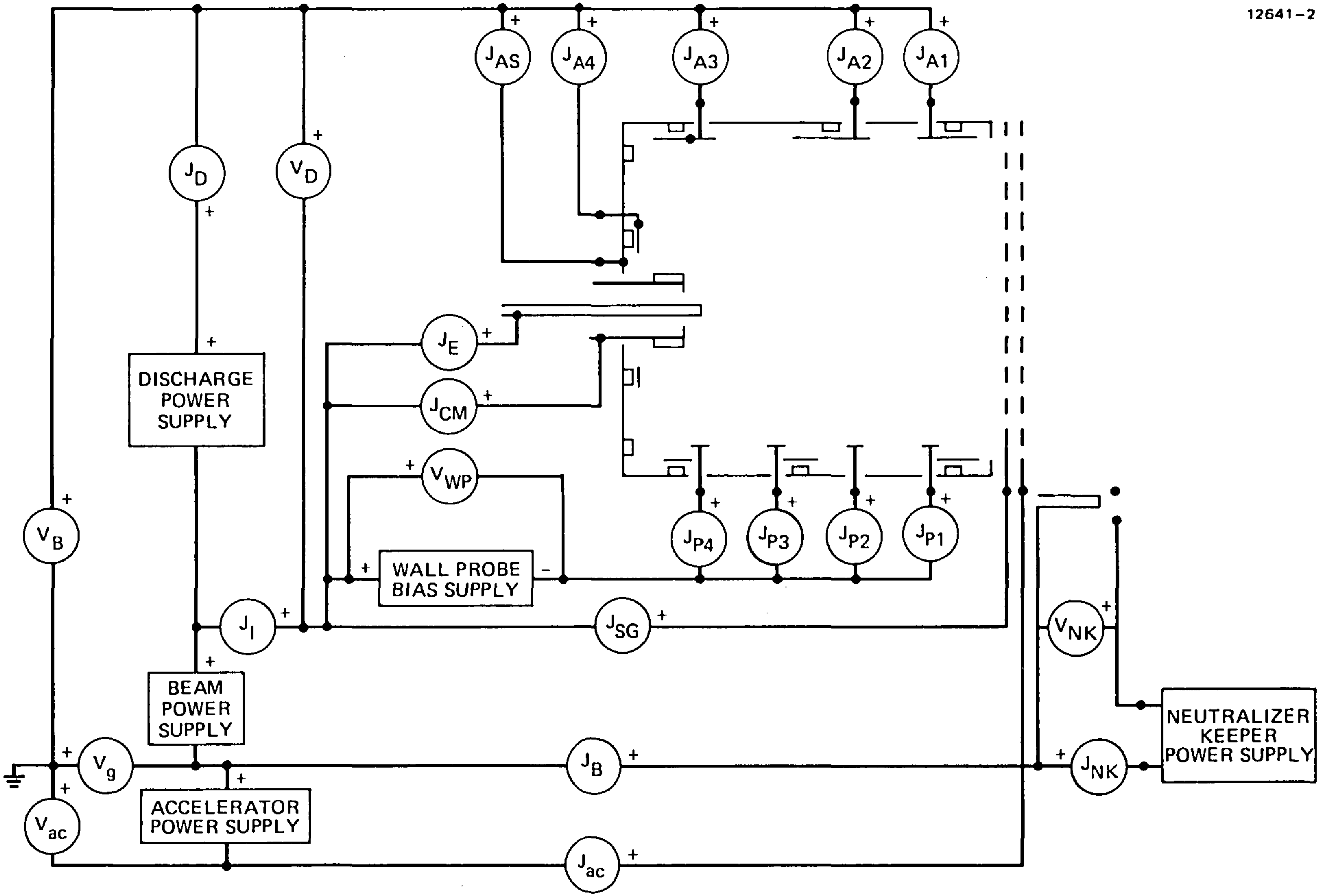

Figure 8. Thruster circuit elements showing voltage and current symbols.

and

$$F = \gamma J_B \left(\frac{2 m_i V_B}{e} \right)^{1/2} , \qquad (10)$$

where g_o is the gravitation constant, e is the electronic charge and m_i is the mass of a propellant atom. Equations (1) through (10) are the basic equations used for determining thruster performance.

B. THRUSTER PERFORMANCE

Operation of ring-cusp thrusters has produced state-of-the-art efficiencies with good reproducibility in several thruster diameters. Although the initial investigation of ring-cusp thrusters was performed at NASA-LeRC, it is notable that equivalent performance has been demonstrated by Hughes using a slightly different hardware design in which the cusp orientation was modified slightly to achieve the same magnetic field distribution. Thruster evaluation was conducted in four phases. The initial tests were performed in the Hughes Research Laboratories facilities where the pumping capacity was not sufficient to permit extraction of an ion beam.

1. Initial Tests at Hughes Research Laboratories

Initial tests concentrated on verifying the stability of the ring-cusp discharge over the range of voltages and currents required to demonstrate the performance goals using argon propellant. For these tests, the screen and accel grid were biased at 20 V negative with reference to the cathode, and the ion current collected on these grids was interpreted as being equivalent to the extracted ion beam. An example of the data obtained in this type of testing is shown as Figure 9. The wall probes were also biased at 20 V negative with reference to cathode potential to collect the currents shown in Figure 9. It is noteworthy that 80 percent of the discharge current (electrons collected) is collected at anodes No. 1 and No. 2 (the principal side-wall cusps), and that the largest

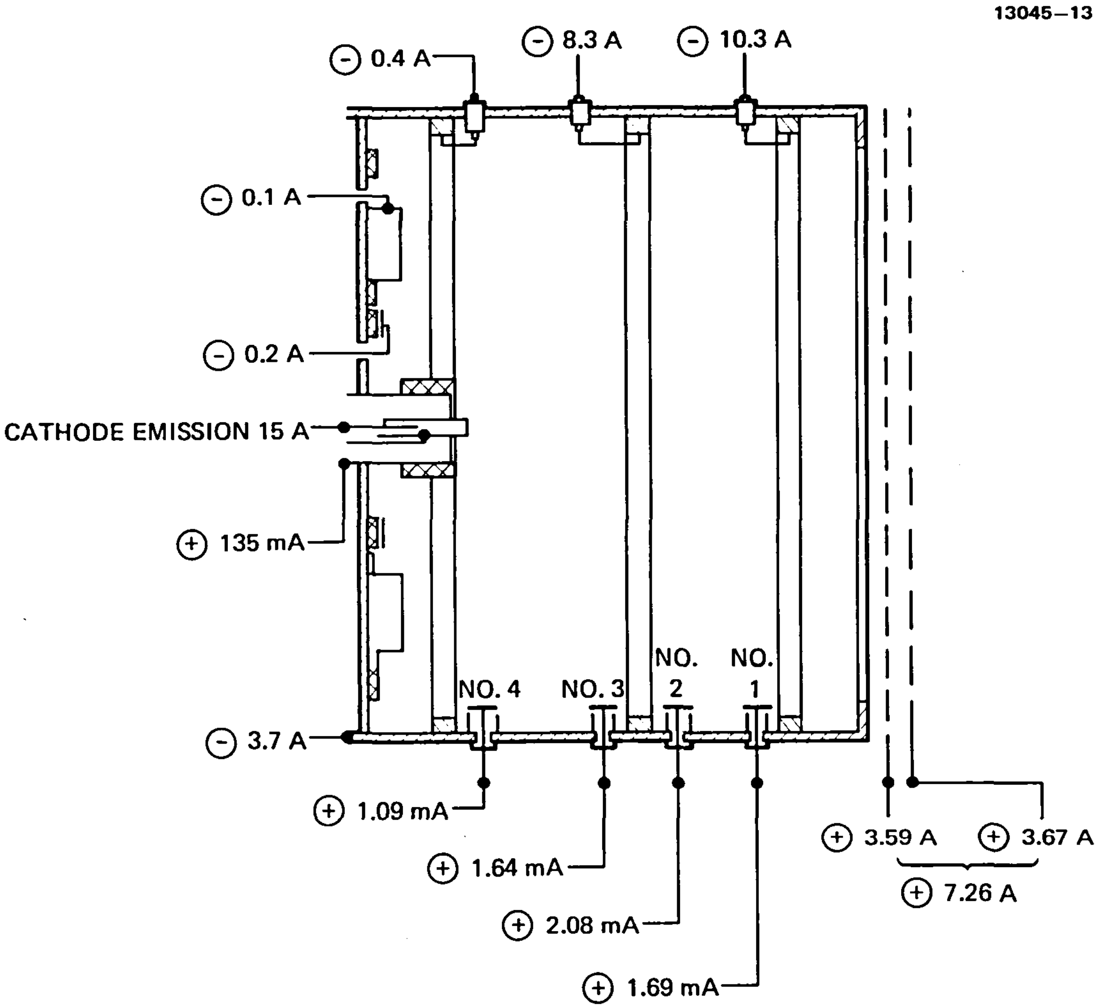

NOTES:

⊖ - ELECTRON CURRENT COLLECTED

⊕ - ION CURRENT COLLECTED

- ANODE VOLTAGE = 40 V
- SCREEN AND ACCEL GRIDS BIASED AT -20 V WITH REFERENCE TO CATHODE POTENTIAL
- ϵ_I = 83 W/A

Figure 9. Distribution of currents collected on discharge chamber surfaces and probes in preliminary test (argon propellant).

portion of this current is collected at anode No. 1. The largest value of ion current toward the sidewall, however, is collected on wall-probe No. 2. If one were to assume that this maximum probe current (wall-probe No. 2) represented the average ion flux to all anode potential surfaces, then the ion current to the side and end walls would amount to about 2.6 A. In combination with the ion currents collected on the cathode magnet and ion acceleration assembly, the total ion production would be about 10 A, which would infer a discharge ion production cost of $\varepsilon_I = 60$ W/A. This line of reasoning also infers that more than 70 percent of the ions produced leave the discharge volume at the ion extraction screen boundary, even though that boundary represents only 10 percent of the area that bounds the discharge-chamber volume. The quantitative values of the ion production and loss as derived in this manner are certainly inaccurate and require refinement; however, the points to be made by this calculation are:

- Ion loss from the discharge plasma is not isotropic.
- The ring-cusp discharge configuration produces an ion drift that is favorable for beam extraction.

To determine the ion flux distribution toward the extraction screen, the ion extraction grid was replaced by a single grid (accelerator-grid hole pattern) that had probes mounted with the collecting surface about 1 mm downstream of the grid. These probes had the same collecting area as the wall probes; however, they were 'masked' by the 20-percent-transparent grid. The probes were located on centerline, and at one-fourth, one-half, and three-fourths beam radii, as shown in Figure 10. The probe currents obtained by operating the discharge chamber with 600 W input power are also shown in Figure 10. In obtaining these measurements it was initially thought that a greater accuracy would be obtained by maintaining the extraction screen probes at cathode potential. Unexpectedly, the centerline probe collected a net electron current even though all other probes collected ion current. With the

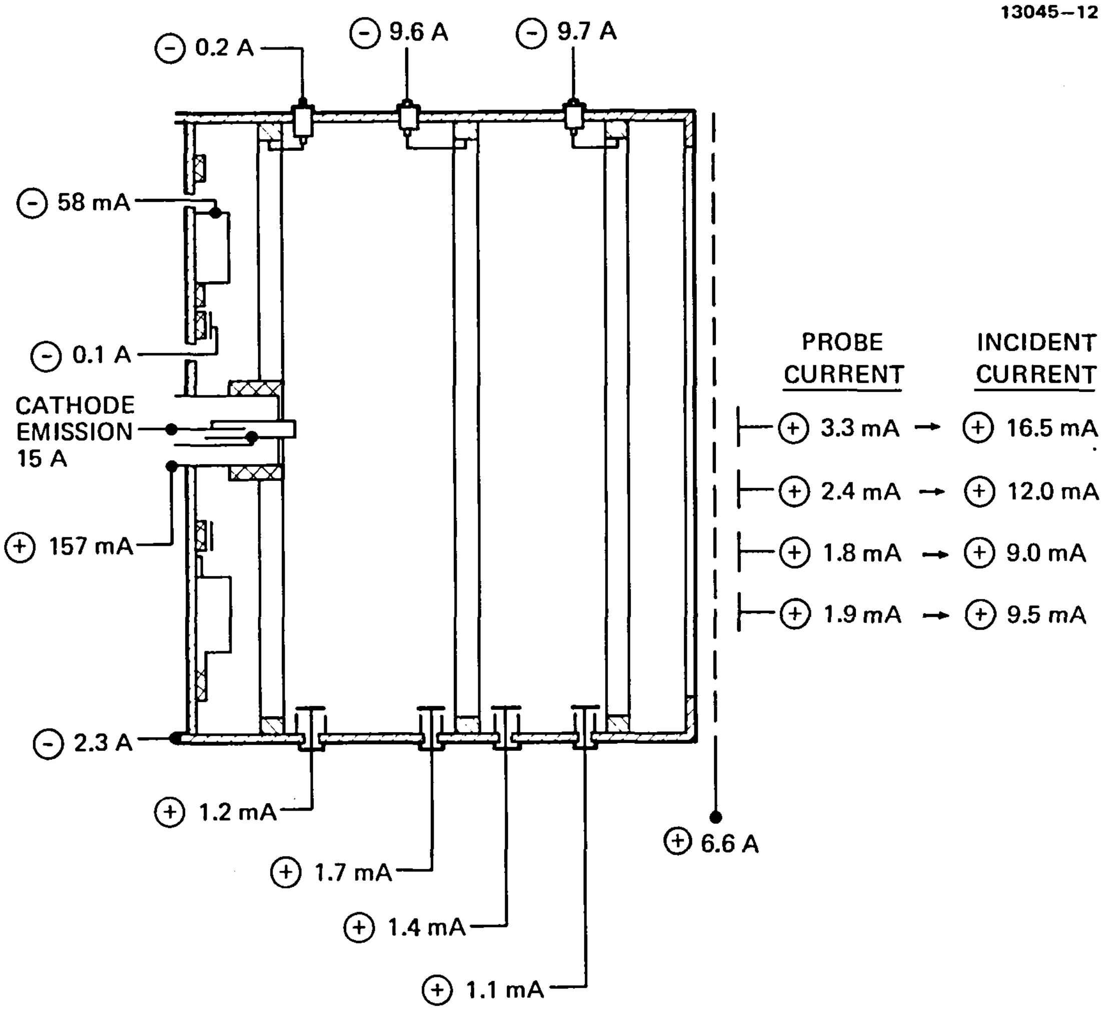

NOTES:

⊖ - ELECTRON CURRENT COLLECTED

⊕ - ION CURRENT COLLECTED

- ANODE VOLTAGE 40 V
- EXTRACTION SCREEN AND ION COLLECTION PROBES BIASED AT -20 V WITH REFERENCE TO CATHODE POTENTIAL
- PROBE CURRENT = 0.2 x INCIDENT CURRENT
- ϵ_I = 91 W/A

Figure 10. Distribution of currents collected on discharge chamber surfaces and probes for discharge chamber equipped with extraction screen probes (argon propellant).

extraction grid biased at -20 V, the centerline probe had to be biased to -30 V (with reference to cathode potential) to obtain ion saturation.

The measurements performed in this first phase of ring-cusp thruster evaluation verified the potential for excellent performance, and disclosed some unanticipated properties of the discharge plasma. The current distributions and discharge plasma properties indicated by the measurements shown in Figures 9 and 10 will be shown to be unrepresentative of the ring-cusp thruster discharge properties that exist when the thruster is operated "normally" with ion beam extraction at near optimum conditions.

2. Initial Tests at the NASA-Lewis Research Center

The second phase of the program was performed at NASA's Lewis Research Center where thruster operation could be performed over a wide range of operating conditions to provide a complete evaluation of the thruster. Data were obtained at over 100 operating points using three ion-extraction assemblies and argon propellant to perform these tests. Some of the operating points were repeated to establish their validity. Initial testing was performed at conditions similar to those used in the Hughes tests, without beam extraction.

Figure 11 gives an example of the current distributions measured in the lower ambient pressure conditions that exist in the LeRC facility for operation with, and without ion beam extraction. The operating point was established with ion beam extraction using Grid Set A (described earlier), and then the extraction voltages were removed and screen and accel electrodes were connected to a bias supply to provide -20 V with reference to the cathode. The propellant flow was constant for these two operating conditions, yet the total ion current produced is significantly less for the operating condition with an extracted ion beam. The electron current collected is also less for the

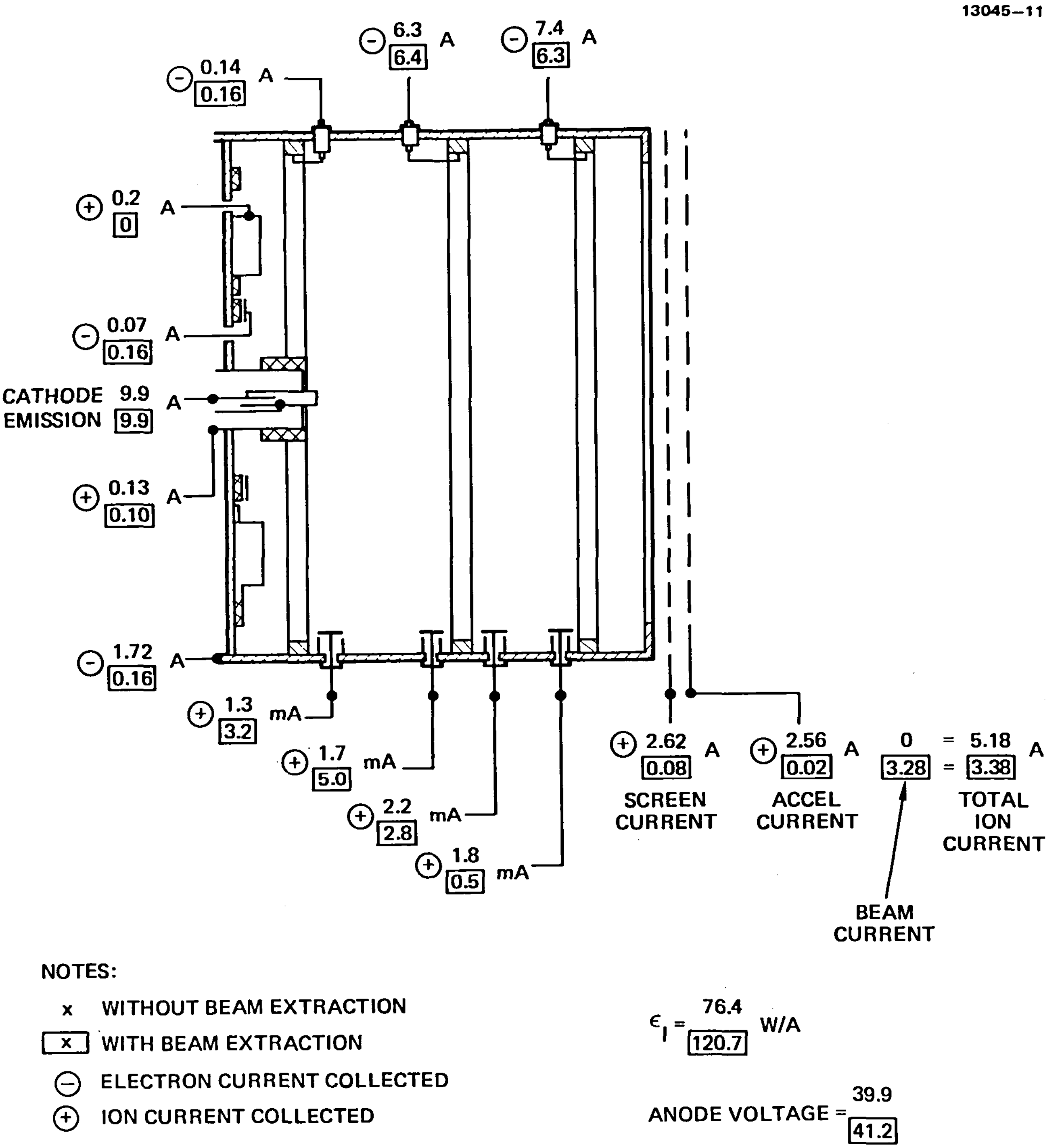

Figure 11. Distribution of currents collected on discharge chamber surfaces and probes for operation with, and without, ion beam extraction. Grid Set A.

operating condition with ion beam extraction, and it appears that the plasma production volume may be centered closer to the cathode end of the discharge chamber for this condition. Although Grid Set A had been tested with beam currents in excess of $J_B = 2$ A with mercury propellant, severe arcing occurred when the thruster was operated at $J_B = 4$ A using argon propellant. When the thruster was operated with Grid Set B, the distribution of currents obtained was changed radically.

Figure 12 compares the distribution of currents collected under similar operating conditions using Grid Set A with those obtained using Grid Set B. Except for the cathode magnet and the ion extraction screen grid, all surfaces appear to collect a net electron current when the thruster was operated with Grid Set B and the ion production cost was reduced to $\varepsilon_I = 104$ W/A. The type of current distribution shown in Figure 12 for Grid Set B is representative of all the data obtained with the thruster operated to obtain $\varepsilon_I \sim 100$ W/A, $\eta_{MD} \geq 80$ percent. Operation of the ring-cusp thruster with Grid Set C produced the best performance.

Figure 13 compares representative discharge chamber performance characteristics for the laboratory model ring-cusp thruster operated with the 3 ion extraction assemblies. The superior performance obtained with Grid Set C is attributed to the higher screen grid transparency obtained using hexagonal shaped apertures. Distribution of currents for operation with this grid set are listed in Table 3.

The distribution of ion current in the extracted ion beam (as a function of radius) was measured using a negatively biased planar probe that traversed the beam in a plane approximately 5 cm downstream of the accel electrode. The thruster was operated at a beam current of about $J_B = 5$ A using Grid Set C to obtain the distribution shown as Figure 14. The current calibration was established by integrating

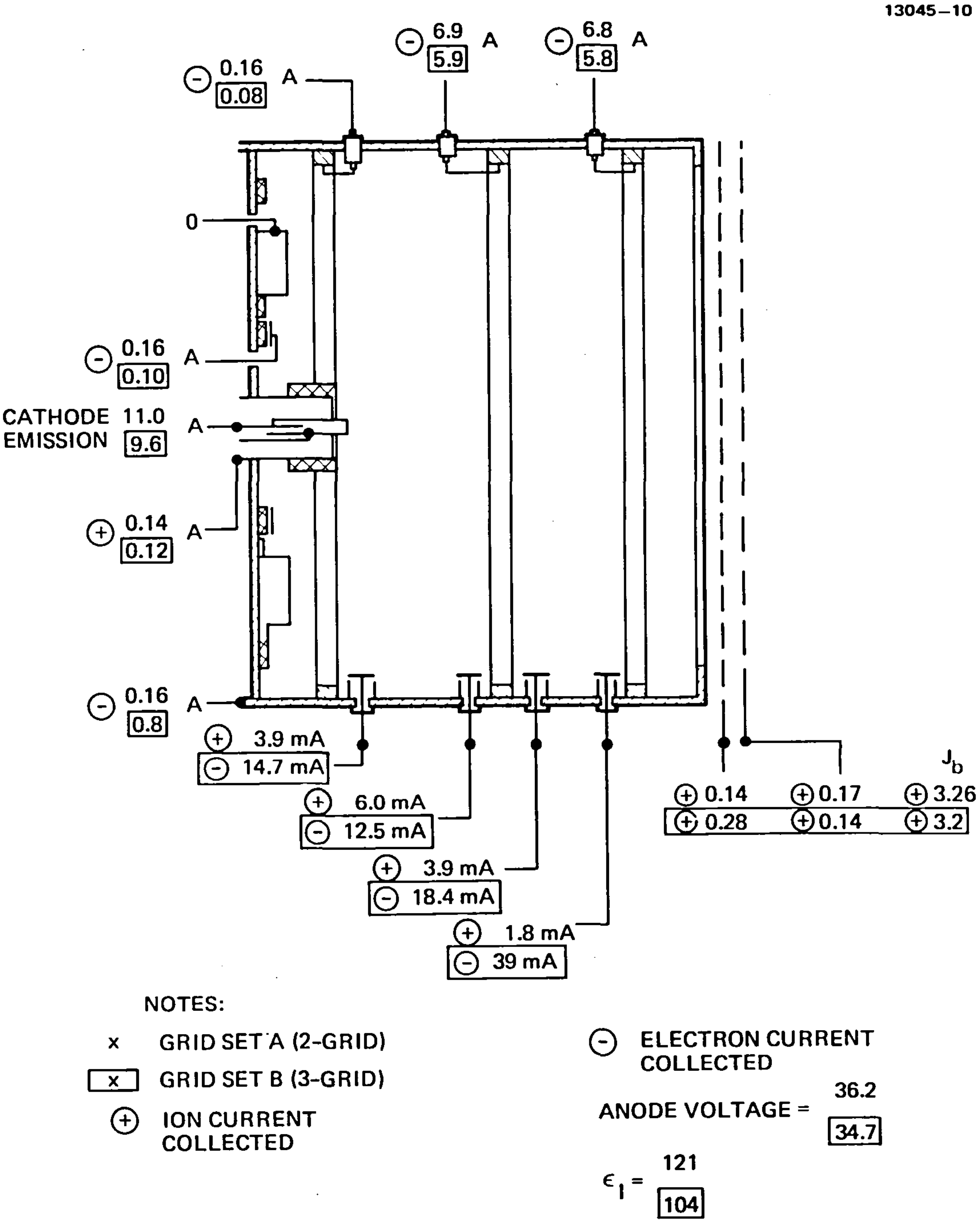

Figure 12. Comparison of discharge chamber electrode and probe currents for operation with different ion optics assemblies.

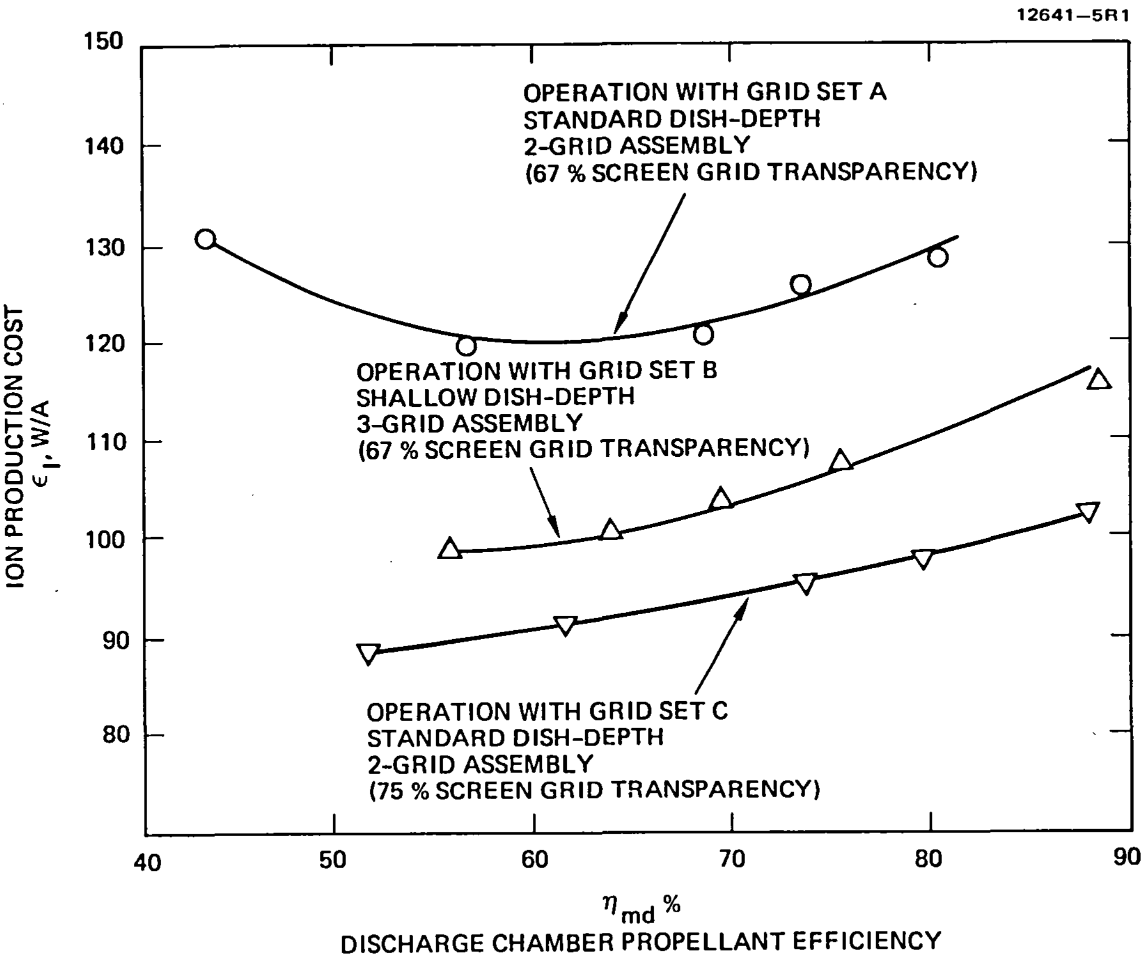

Figure 13. Comparison of discharge chamber ion production cost characteristics for operation with 3 ion extraction assembly designs.

Table 3. Examples of Discharge Chamber Electrode and Wall Probe Currents Under Conditions of Efficient Discharge Chamber Operation Ⓐ

J_B , A	4.0	5.1	6.0
V_D , V	40.9	40.2	40.7
J_I , A	10.1	13.0	15.0
ε_I W/A	103	102	102
η_m %	85.2	86.3	84.8
J_{P1} , mA Ⓑ	-8.4	-11.3	-9.9
J_{P2} , mA	-11.3	-9.3	-6.0
J_{P3} , mA	-3.8	-3.3	-1.8
J_{P4} , mA	-6.7	-9.1	-5.0
J_{SG} , A	+0.06	+0.04	0.0
J_{CM} , A	+0.12	+0.14	0.18
J_{A1} , A	6.8	9.3	7.1
J_{A2} , A	6.4	8.0	9.0
J_{A3} , A	0.06	0.06	0.08
J_{A4} , A	0.08	0.08	0.10
J_{A5} , A	0.02	0.6	4.5

Ⓐ Grid Set C.

Ⓑ $V_{WP} = 0$, negative current indicates electrons collected.

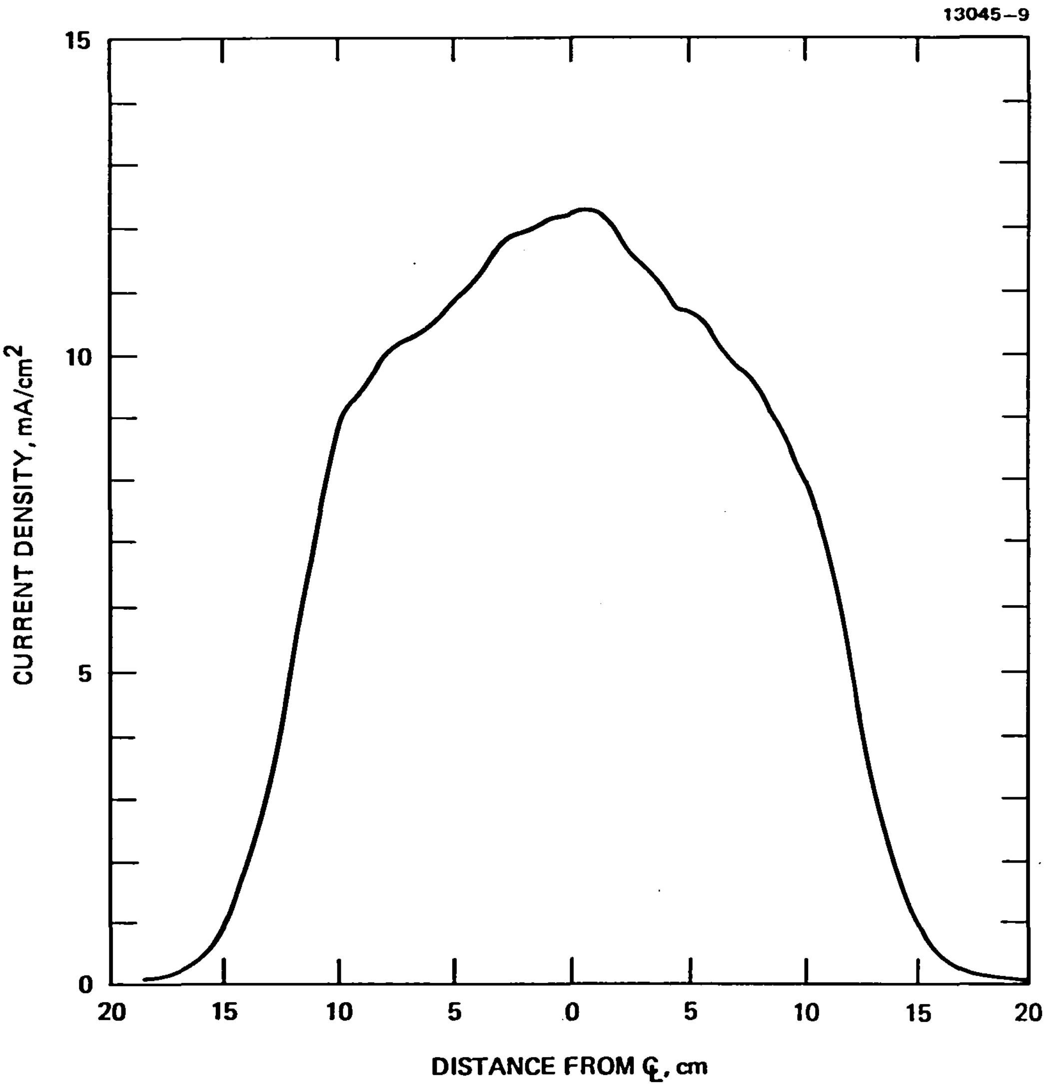

Figure 14. Current density distribution measured in the extracted ion beam of the laboratory model ring-cusp thruster operated with Grid Set C.

the distribution to produce the measured beam current. The flatness parameter computed for this distribution is 0.54. While this value of the flatness parameter is considered to represent a relatively "peaked" current distribution, it is an improvement over the NASA/Hughes 30-cm-diameter J-series mercury ion thruster which has a flatness parameter of about 0.47. If the interior plasma density distribution has the same radial dependence as the current distribution of Figure 14, then the plasma density drops sharply at a radius of 10 cm. Referring to Figure 7, the 10-mT equimagnitude contour would define a cylinder of about 10-cm radius. This 10-mT contour may prove to be a valid measure for defining the plasma boundary.

The measured discharge performance and beam current have been used to prepare Table 4 for projection of the performance characteristics of the ring-cusp thruster that would be attainable using a 3-grid ion extraction assembly to operate at several values of specific impulse. To project the overall thruster performance, the formulas in the footnotes of the table were used. These formulas represent an approximation to the best operating conditions that were achieved in mapping the neutralizer characteristics. By using these expressions to compute an overall propellant efficiency, we were able to calculate the beam voltage required to obtain the specific impulse noted for each entry. The beam power and total power was then calculated to obtain the overall thruster efficiency and corrected thrust. Note that for each value of specific impulse, the value of beam current, ion production cost and discharge propellant utilization are repeated. These data points are considered to be well established and repeatable. The last set of performance data shows variation in specific impulse from I_{sp} = 3690 sec at a beam current, J_B = 6.5 A, to I_{sp} = 2320 sec at J_B = 3.0 A. The specific impulse values are the minimum achievable maintaining the value of the net-to-total accelerating ratio, R, at $R \geq 0.3$. It is noteworthy that the efficiency at any constant value of specific impulse remains more or less constant as the power (thrust) level is decreased. This characteristic is a departure from the reduction in efficiency usually observed when the power level of an ion thruster is reduced.

Only one datum point was obtained operating with xenon propellant. Extrapolating performance characteristics from this datum point yields the performance characteristics shown in Table 5. In this case, the actual datum point provided the beam current, ion

Table 4. Performance Characteristics for a 30-cm Diameter Ring-Cusp Thruster Operated on Argon

J_B A	I_{SP} sec	P_B W	Ⓐ P_{TOT} W	V_D V	ε_I W/A	η_{MD} %	Ⓑ η_T %	F mN	F/P, mN/kW
6.5	6000	8236	9145	42.5	106	85.3	66.5	207	22.6
6.0		7602	8417	40.7	102	84.8	66.7	191	22.7
5.0		6505	7186	40.3	102	86.3	66.0	161	22.4
4.0		4940	5492	40.9	103	85.2	67.4	126	22.9
3.0		3903	4319	42.2	103	83.2	65.9	97	22.4
6.5	5000	5720	6640	42.5	106	85.3	63.6	173	26.2
6.0		5280	6103	40.7	102	84.8	63.9	159	26.1
5.0		4515	5196	40.3	102	86.3	63.3	134	25.8
4.0		3432	3979	40.9	103	85.2	64.3	105	26.4
3.0		2709	3121	42.2	103	83.2	63.2	80	25.6
6.5	4000	3660	4592	42.5	106	85.3	58.9	138	30.0
6.0		3378	4213	40.7	102	84.8	59.2	127	30.1
5.0		2890	3581	40.3	102	86.2	58.8	108	30.2
4.0		2196	2751	40.9	103	85.2	59.7	84	30.5
3.0		1734	2148	42.2	103	83.2	58.8	65	30.2
6.5	3690	3120	4056	42.5	106	85.3	56.8	127	31.3
6.0	3600	2742	3580	40.7	102	84.8	56.5	115	32.1
5.0	3340	2020	2716	40.3	102	86.3	54.2	90	33.1
4.0	3190	1396	1956	40.9	103	85.2	53.4	67	34.2
3.0	2820	861	1280	42.2	103	83.2	49.0	45	35.2

Ⓐ $P_{NK} = 8$ W, $V_g = 30$V, $P_{ac} = 0.006\ J_B V_{ac}$ W

Ⓑ $\gamma = 0.98$, $m_N = 0.12\ J_B$, A,
Vacuum Facility Pressure: 1.6×10^{-3} Pa to 2.8×10^{-3} Pa or 1.2×10^{-5} Torr to 2.1×10^{-5} Torr; propellant flow corrected for back-flow ingestion.

Table 5. Performance Characteristics for a 30-cm Diameter Ring-Cusp Thruster Operated on Xenon

J_B A	I_{SP} sec	P_B W	Ⓐ P_{TOT} W	V_D V	ε_I W/A	η_{MD} %	Ⓑ η_T %	F mN
4.5	3060	3600	4128	32	100	96	77.0	206
3.5	3030	2800	3212	32	100	96	76.2	160
2.5	2966	2000	2298	32	100	96	74.4	114

Ⓐ P_{NK} = 10 W, V_g = 15 V.

Ⓑ γ = 0.98, m_N = 0.2 A,
Vacuum Facility Pressure: 2.0 x 10^{-3} Pa (1.5 x 10^{-5} Torr).

production cost, and discharge propellant utilization for the J_B = 2.5 A entry. Again, the neutralizer performance is projected using the expressions shown in the footnotes of Table 5. The data in Tables 4 and 5 are considered to be representative of the performance attainable with the 30-cm ring-cusp thruster configuration as defined earlier. With the completion of the tests in the NASA-LeRC facilities to produce this data, the first two phases of ring-cusp thruster development under this program were completed. Excellent thruster performance have been demonstrated and the performance characteristics have been documented.

3. Data Analysis and Correlation

Emphasis for the later phases of development under this program was focused on providing analysis and diagnostic measurements that would aid in defining the design or operational parameters that are critical for achieving the superior performance characteristics already demonstrated. The third phase of the program was conducted at Hughes Research Laboratories and consisted primarily of analyzing and correlating results already obtained and in performing additional measurements to better explain observed behavior. The diagnostic techniques required for the final tests in the NASA-LeRC facilities were also determined, prepared and refined. The outstanding question that had to be answered concerned the factors that influence or control ion flux to the discharge chamber boundaries.

To address this question, it was relatively obvious that Langmuir-probe measurements would have to be made; however, achieving representative operating conditions at the Hughes facility presented a problem. As illustrated earlier in Table 3, the net current collected at the wall probes undergoes a transition from ion current to electron current when the discharge is operated under conditions that produce superior thruster efficiency. The ion current collected on the ion extraction screen was also observed to decrease under operating conditions that produce high propellant utilization and good ion production efficiency. In some cases, a net electron current was also observed at the screen grid (note that the wall probes and screen grid were operated at cathode potential under these conditions). Applying a bias voltage to the wall probes to obtain a net ion current (during LeRC tests) required a negative voltage of 12 V for WP3 (see Figure 15), and a net ion current could not be obtained at WP1 and WP2, even with a negative 15 V bias (limited by power supply provided). No means could be found under "discharge-only" operation (without extracting an ion beam) to reproduce these results. Another similar observation can be made in reference to the plasma density distribution as inferred from measurement of the radial current distribution in the extracted ion beam (Figure 14). The plasma distribution is significantly different from the distribution inferred from the current measured with the screen probes (shown earlier in Figure 10). Figure 16 compares these distributions as they appear when normalized to the axial current density. The point to be made is that in order to

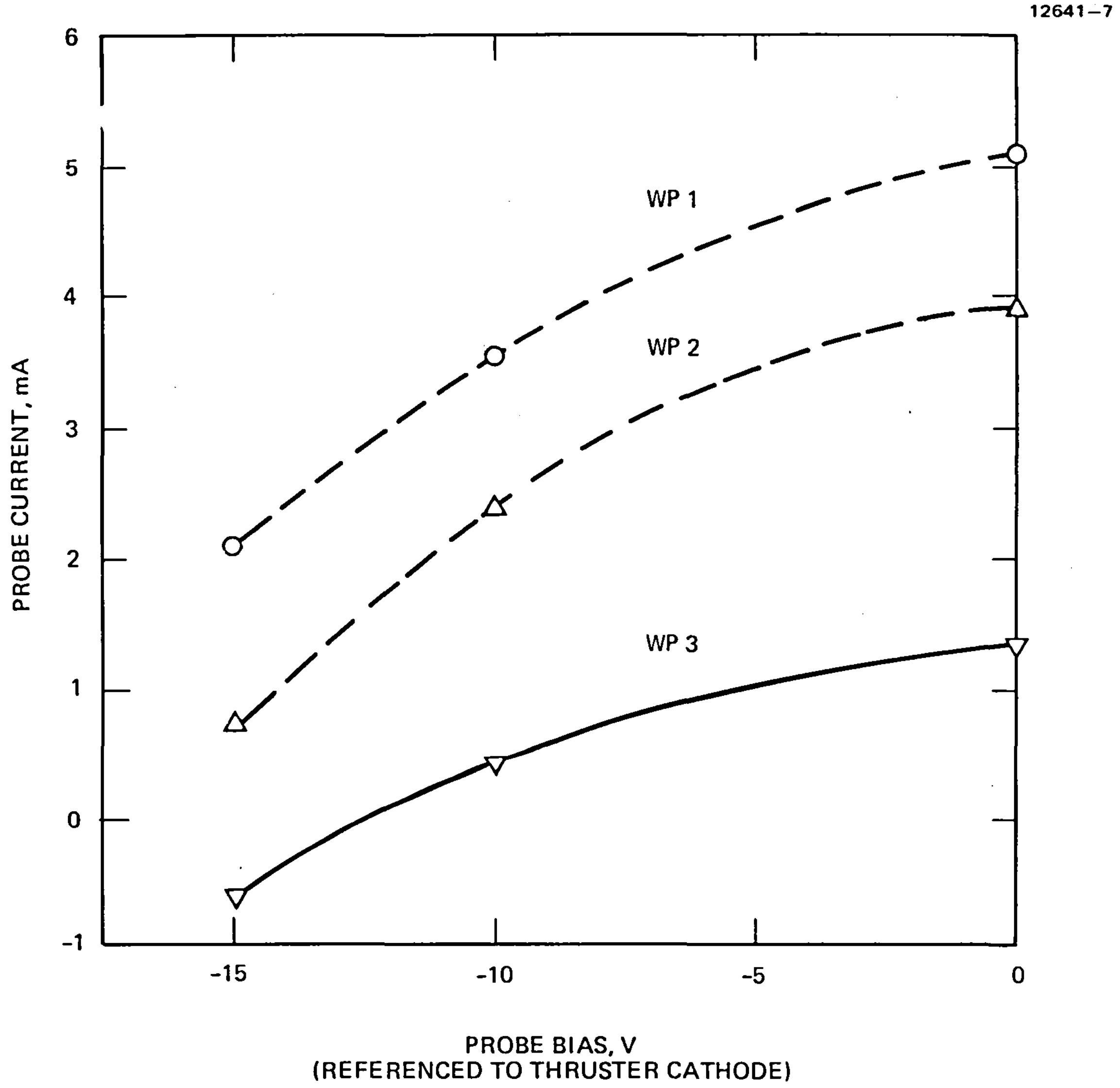

Figure 15. Wall probe current as a function of wall probe bias (positive current corresponds to electron collection).

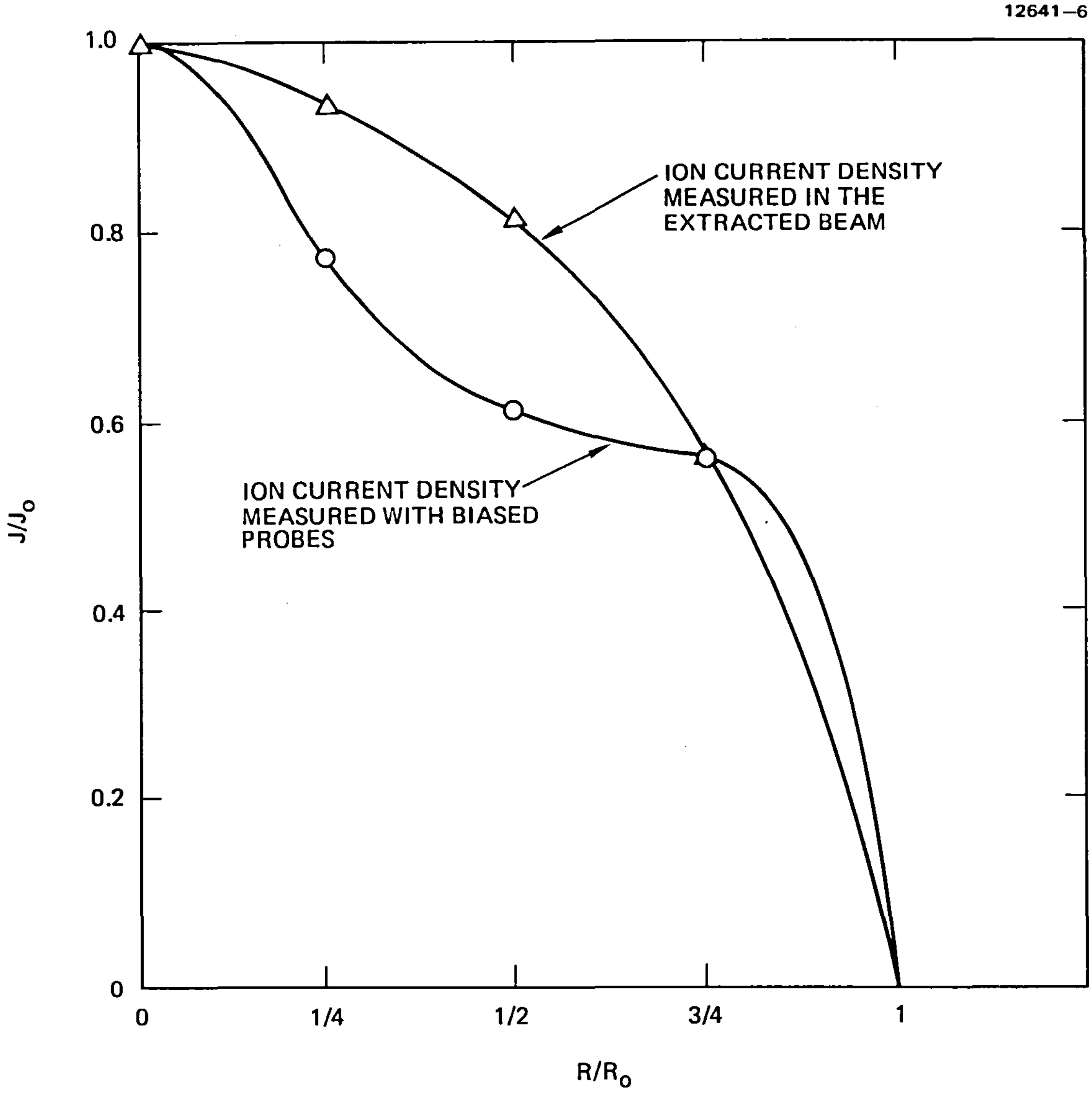

Figure 16. Modification in ion current density distribution collected at the screen grid when an ion beam is extracted from the discharge chamber.

provide a meaningful description of discharge plasma properties (such as spatial density distributions and resultant density gradients), diagnostic measurements have to be performed under normal thruster operating conditions with representative ion beam extraction.

A quasi-steady mode of pulsed thruster operation was devised to operate the 30-cm ring-cusp thruster on inert gases with representative beam extraction. A description of the methodology and characteristics of thruster operation under pulsed-mode operation will be presented in the Advanced Technology section. Some insight into plasma processes was gained in pulsed-mode operation using argon propellant. The thruster was operated with an extracted ion beam up to $J_b = 5$ A, over the normal range of discharge currents and voltages, and with representative ion production costs. Langmuir probe data were taken to explore the effects of beam extraction and to characterize plasma potential, electron energy, and plasma density. Although some preliminary results were obtained in pulsed-mode generation the validity of these results as being representative of normal thruster operation is still in question. For example, the collection of electron current by either the wall probes or the extraction grid (screen grid) was never observed in pulsed-mode operation. A major difficulty which we did not attempt to solve was a problem in maintaining pulse-to-pulse repeatability for more than a few successive pulses without readjusting power supplies. But operation in pulsed mode did enable us to check our Langmuir probe and probe circuitry under beam extraction conditions. Moreover, the pulsed-mode plasma properties at the location of the stationary probe were in relatively good agreement with those measured in the final experiments at the NASA-LeRC facility. These initial measurements disclosed two features of the ring-cusp thruster discharge-chamber plasma that have been found to occur for nearly all operating conditions. First, the plasma potential is essentially the same as the anode potential, and second, the electron energy distribution is essentially "Maxwellian", with an electron temperature ranging from 5 V < T_e < 12 eV. A comparison for pulse-mode Langmuir-probe results with results obtained by continuous operation with and without ion extraction is provided in Table 6. A representative Langmuir probe characteristic is shown in Figure 17. The location of the Langmuir probe for all measurements was shown earlier in Figure 7.

Table 6. Comparison of Plasma Properties Measured in Continuous-Mode Operation and Pulsed-Mode Operation with Ion-Beam Extraction, and in Continuous Mode Operation Without Beam Extraction

Property	Mode of Operation		
	Continuous	Pulsed	Continuous
Beam current, A	1.51	1.5	0.0
Discharge voltage, V	40.7	40	38.4
Plasma potential, V	41.0	43	37.8
Electron Temperature, eV	6.0	6.0	4.3

4. Final Tests at the NASA-Lewis Research Center

The final experiments in the NASA-LeRC test facility and the subsequent analysis of data comprised the fourth phase of the program. Rather unexpectedly, there was a loss in performance in the last phase of testing that was eventually attributed to the insertion of the metal-sheathed Langmuir probe into the discharge and through the high-field-strength region between the major electron-confinement magnetic cusps. The probe sheath was approximately 5 mm in diameter and appears to have had a significant perturbing effect. Table 7 compares several discharge chamber operating characteristics for similar ion extraction and propellant flow conditions. Our interpretation is that ions are lost to the

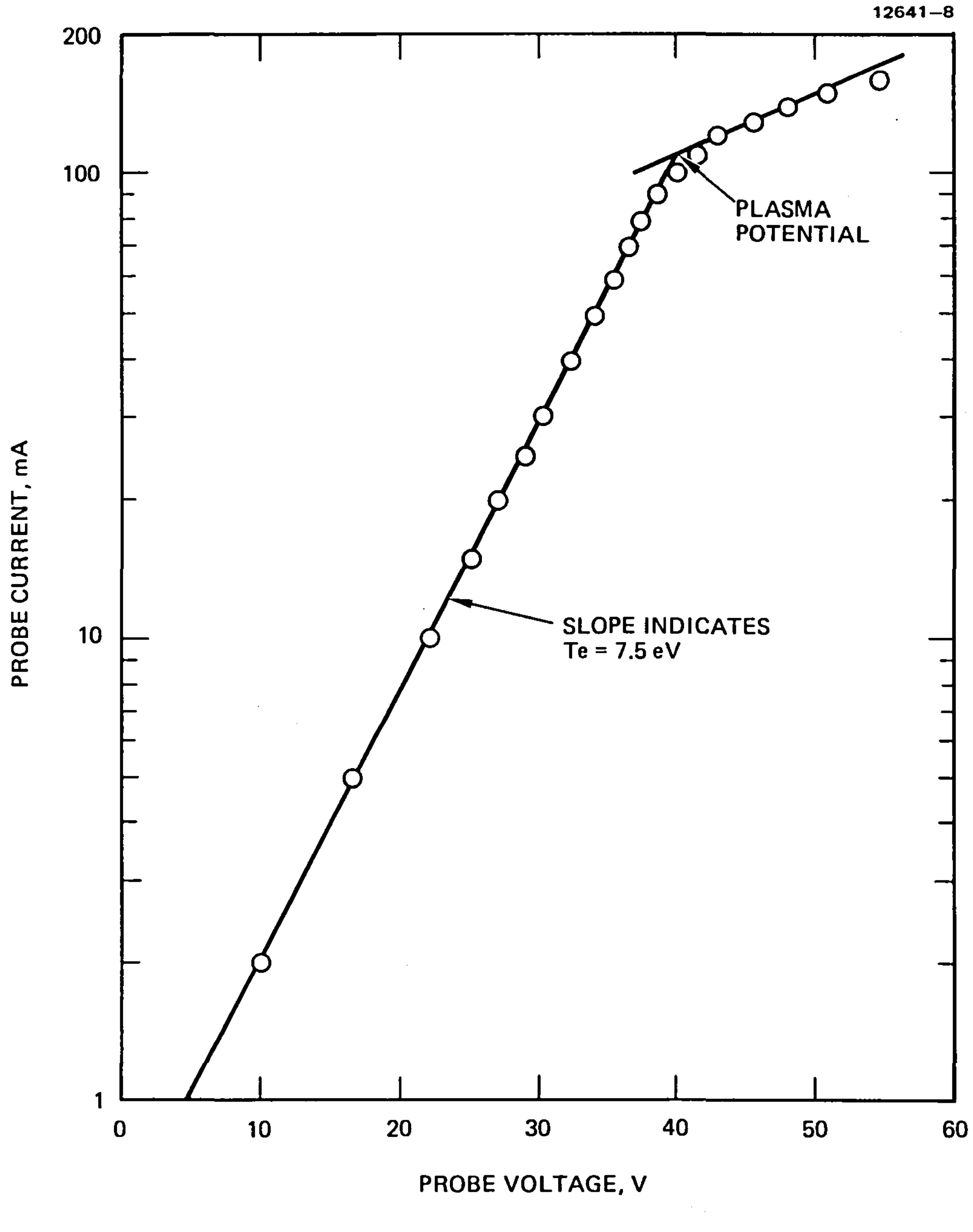

Figure 17. Langmuir probe voltage/current characteristic for thruster operating conditions listed in Table 6.

Table 7. Perturbing Effect of Langmuir-Probe on Discharge Properties

Probe Sheath Potential	Cathode	Floating	No Probe
Discharge voltage, V	41.1	38.7	37.9
Discharge current, A	16.9	15.1	13.6
Beam current, A	5.49	5.35	5.31
Discharge loss, W/A	126	109	96.9
Screen grid current, A	0.38	0.33	0.02

probe sheath in sufficient numbers to degrade performance because the loss to other discharge chamber boundaries is relatively small. When the probe sheath and probe were allowed to float, fewer ions were lost. However, the presence of the probe was still a perturbation. Because of this perturbation, the measurement of a predominantly Maxwellian electron energy distribution may also be in error, since any high energy or "primary" electron constituent may be eliminated because of the probe. This effect will have to be explored further before the validity of the plasma properties measured can be verified.

Whereas we had expected to discover either a high energy component of electrons in the discharge or an extremely depressed plasma potential, neither of these conditions were observed. Plasma electron temperature and plasma potential are both closely correlated with the discharge (anode) voltage, but the plasma properties were not found to be "unusual" in any respect except for the absence of a monoenergetic component of electrons with energy corresponding to the discharge voltage. Figures 18 and 19 show the correlation of plasma electron temperature and potential with the discharge voltage. While there is some scatter in the data, an almost linear relationship with discharge voltage exists for these two plasma characteristics.

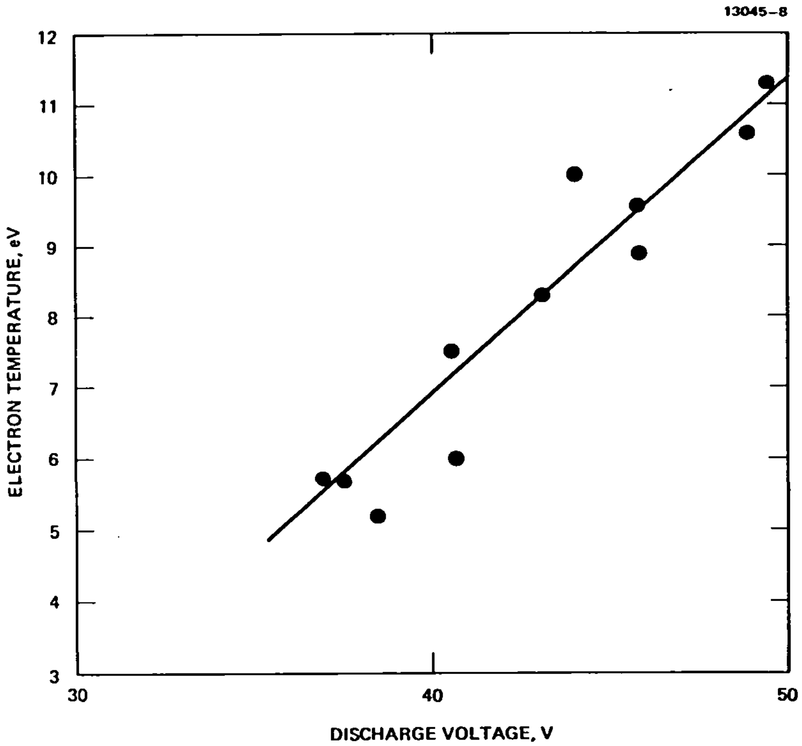

Figure 18. Plasma electron temperature versus discharge voltage.

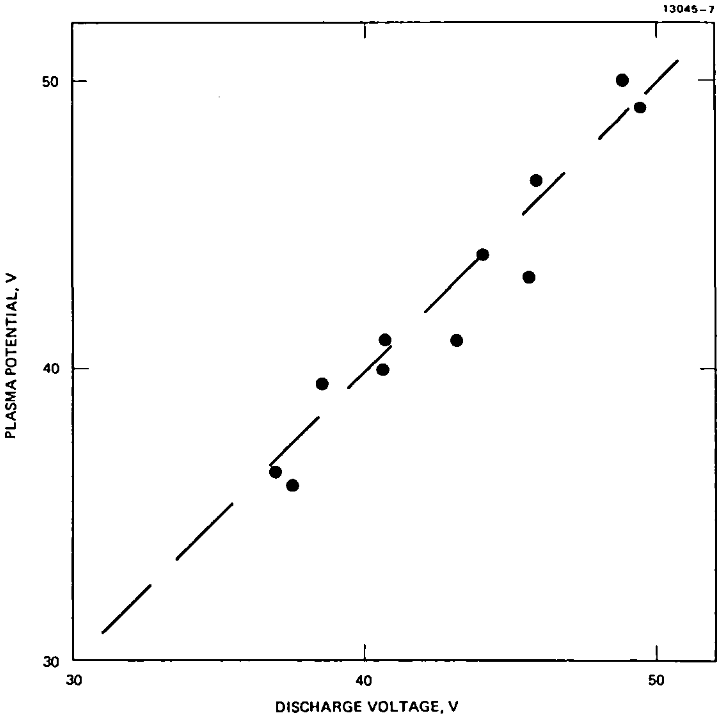

Figure 19. Plasma potential, V_p, versus discharge voltage.

C. DISCUSSION OF RESULTS

Experimental measurements obtained with the ring-cusp thruster infer a relatively low volume-ion-production cost and efficient ion containment. The Langmuir probe measurements did not indicate a sufficient depression in the plasma potential to establish a meaningful argument for electrostatic containment.[5] Nevertheless, the measurements were all obtained at a single location and, therefore, local "ridges" in plasma potential cannot be ruled out. Moreover, wall-probe measurements show that ion current flows to all surfaces in some quantity under most operating conditions and, therefore, ion containment, in an absolute sense, is not in evidence. All experimental observations point to a plasma that is generated and contained in a manner such that the ions drift preferentially toward the ion extraction screen. An explanation and theoretical analysis of the condition has been described by Kaufman, Robinson, and Frisa,[6] and similar experimental observations have been reported by Brophy and Wilbur.[7] A brief description of their analysis follows.

Figure 20 shows a cross-section of the ring-cusp discharge chamber to illustrate the relation of the magnetic lines of force and the discharge electrodes to an assumed ion (plasma) production region (which is identified by the heavy solid line). The plasma volume is considered to be defined by a surface of revolution of this boundary. Except at the cathode magnet and screen grid boundaries of this volume, the surface is thought to be at anode potential. Because of the strong magnetic field, electrons can reach the physical anode only at the magnet poles, and then only if their velocity vector is oriented so that ion-reflection* does not occur at the cusp. The net-diverging magnetic-field intensity

---

*Ion-reflection can occur at points of magnetic-field convergence because of the adiabatic invariance of the magnetic moment.

12641-17R1

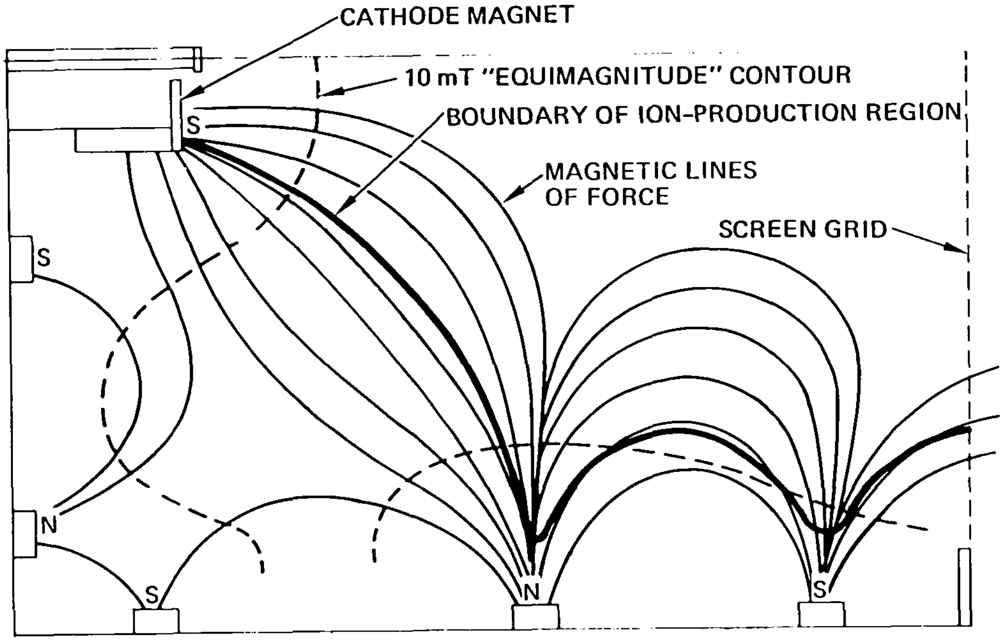

Figure 20. Sketch showing the 30-cm ring-cusp discharge chamber and Hughes estimation of the approximate shape of the boundary of the ion-production region.

serves to move the energetic electrons close to the extraction system and to spread them uniformly over that surface. Since the screen electrode is biased at cathode potential, ions are drawn toward the extraction system and electrons are repelled unless they have gained sufficient energy (from turbulent plasma processes) to overcome the electric field which would otherwise oppose their return to the potential of their origin. The electron spacecharge (or virtual cathode) generated by the electron turn-around, then, sets up a potential distribution which establishes the so-called Bohm pre-sheath which extends deeply into the discharge and accelerates ions toward the extraction system.

The preferential drift direction is explained by Kaufman, Robinson and Frisa[6] by showing that a Bohm sheath is not set up at the discharge-chamber boundaries which are at anode potential. The Bohm pre-sheath condition results directly from the simultaneous solution of Poisson's equation for both ions and electrons subject to the distribution functions for the two species and the necessary plasma condition of quasi-neutrality.[9] They point out, however, that electron loss to an anode-potential surface can severely perturb the electron distribution function and therefore modify the appropriate simultaneous solution to Poisson's equation. Under these conditions, the plasma requirement of quasi-neutrality demands a magnitude for the ion velocity which is well below the Bohm value. Accordingly, ion loss to anode-potential surfaces is similarly reduced. The results of Brophy and Wilbur[7] indicate that ion loss to anode potential surfaces may be consistent with the ions having only thermal velocity.

In the measurements performed under this program, there is no single measurement or experiment that unequivocally verifies controlled or preferential drift of plasma ions toward the extraction screen. By considering all of the experimental evidence in totality, we conclude that there are strong arguments for stating that the ring-cusp thruster investigated here provides control of plasma ion trajectories by limiting radial ion losses and enhancing axial ion losses (by using high transmission ion extraction grids). This control is thought to be a direct consequence of containing the energetic plasma electrons with very strong magnetic fields. We speculate that discharge stability is maintained by the cusp geometry that permits low energy electrons to "leak" out of the containment volume along the magnetic lines of force.

D. DESCRIPTION OF A RING-CUSP THRUSTER CONFIGURED FOR FLIGHT

The laboratory model ring-cusp thruster tested under this program was constructed using relatively thick iron members to form the discharge chamber. For flight hardware, the iron path would have to be constructed of high permeability, relatively thin magnetic members.

Figure 21 shows a drawing of the ring-cusp thruster configured for flight weight and structural qualifications. The inside of the discharge chamber is a continuous cylinder with a closed upstream boundary. Wire mesh is bonded to the interior surface of the anode cylinder except over the magnets. The magnet circuit is constructed of an outer shell assembly with openings to permit the anode heat to be radiated away. The samarium-cobalt magnet is bonded to this assembly with an appropriate fastening (braze) material that has a sufficiently low application temperature to prevent irreversible magnet damage (pure tin is a possibility for which feasibility was shown under the program). Spacer rings prevent the inner anode cylinder from contacting the magnet surface to reduce heat transfer directly to the magnets.

The flight-type-thruster cathode and ion extraction assemblies are identical to those used with the laboratory thruster (derived from the NASA/Hughes J-series mercury ion thruster designs). An igniter electrode is shown for initiation of the thruster discharge even though this may not be required if the discharge supply has sufficient open circuit voltage and high flow rates can be tolerated for ignition. The cathode and cathode magnet are insulated (electrically) from the anode structure using a fully-shielded, machinable-ceramic spacer.

The thruster ground screen, neutralizer, and isolators are not shown. These components and the mounting for the thruster require some further definition of its intended use (i.e., gimbal-mounted, array-mounted, etc.). Viton (fluoroelastomer) tubing served quite well as a propellant electrical isolator in tests of the laboratory thruster and could possibly be acceptable in the eventual application of an inert-gas thruster. These components are considered to be engineering details that will require further specifications for completing their definition, and they were not addressed in detail under the program.

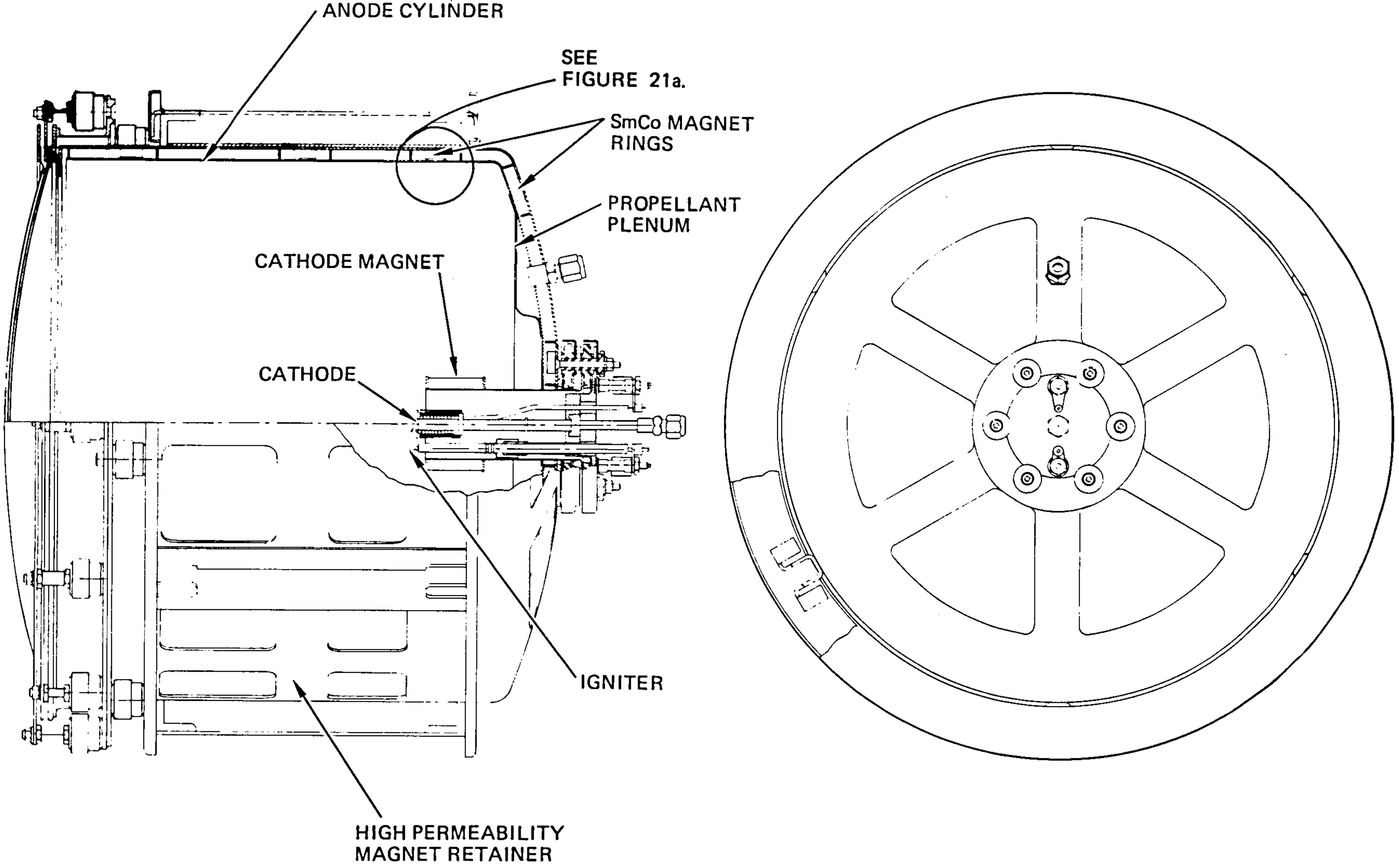

Figure 21. Protoflight ring-cusp thruster drawing.

13014-25R1

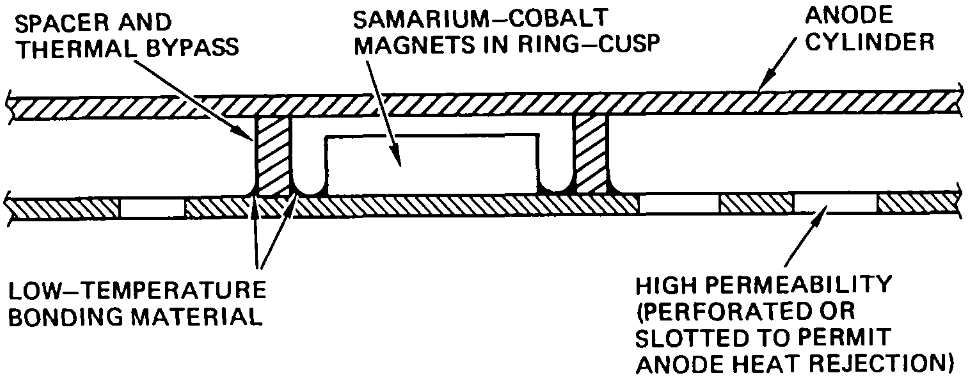

Figure 21a. Magnetic circuit elements and anode cylinder proposed for engineering model thruster designs.

SECTION 3

ADVANCED THRUSTER TECHNOLOGY

While the major achievements under this program were related to the development of the ring-cusp thruster, several sub-tasks were completed that advanced the state of the art for inert-gas thruster technology in general. This section discusses the results of these sub-tasks and their significance in the development of large inert-gas thrusters.

A. OPERATION OF A THRUSTER DISCHARGE CHAMBER WITH TWO HOLLOW-CATHODES

In the design of a thruster for producing 0.5 N of thrust, we initially projected a requirement for thruster discharge currents on the order of 100 A. While it is conceivable that a hollow-cathode could be scaled for operation at this high current value, there was concern about severe ion bombardment of the cathode and its surroundings because of the high plasma density that would be created in the vicinity of such a high emission current if it was provided from a single source. Consequently, a distributed electron source was sought that would be supplied by two or more hollow cathodes. Feasibility was demonstrated under this program for using two cathodes to supply balanced emission to the discharge chamber: the same techniques could also be used to balance emission from more than two cathodes.

To provide a source of electrons that is supplied by two cathodes more or less uniformly through an annular opening, a toroidal electron injection plenum was devised, as shown in cross-section in Figure 22. Emission is divided and balanced between the two cathodes shown by controlling the gas supply in inverse proportion to the electron emission. Valves with fast-response, piezoelectric transducers were used to vary the gas flow. The emission balance was achieved using Hall-current sensors and the

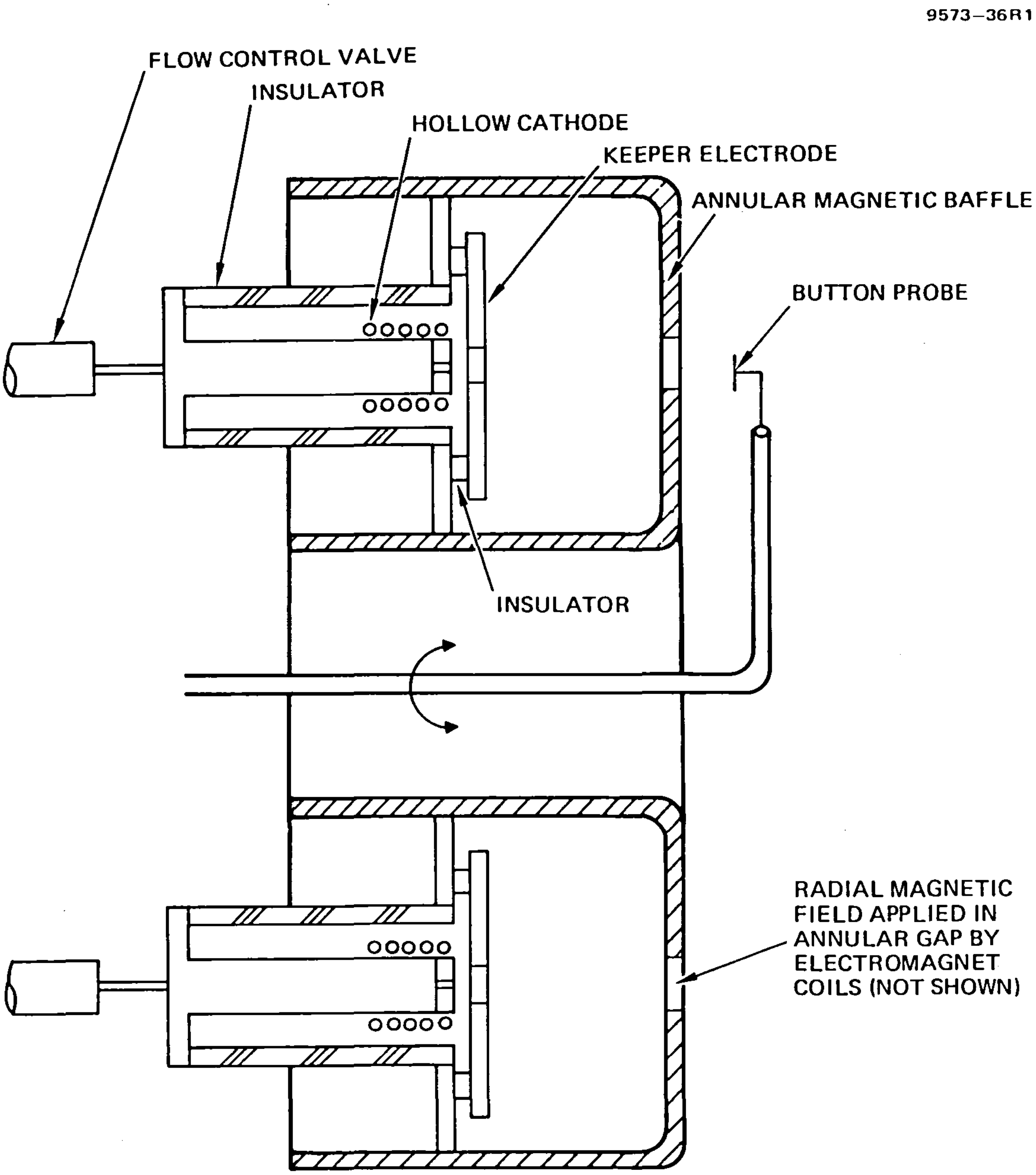

Figure 22. Schematic drawing of the toroidal electron injection plenum for operation of the discharge chamber with two cathodes.

circuitry shown schematically in Figure 23. It was possible to ignite the discharge and maintain both emission balance and discharge voltage control using this circuit to control cathode gas flow to the cathodes under all of the discharge operating conditions that are usually encountered in thruster operation. These conditions include low-discharge-current idling or emission cutback for high-voltage-overload recycle, operation of the discharge chamber without ion beam extraction, and normal operation of the thruster with ion beam extraction. The use of the piezoelectric valves in this application also demonstrates the tractability of using these valves for closed-loop control of all the thruster gas supplies (neutralizer, cathode, and discharge gas flows).

The toroidal electron injection plenum chamber shown in Figure 22 encloses the cathode plasma generated by the two hollow cathodes, and electrons are supplied to the thruster discharge chamber through the annular gap designated as the annular magnetic baffle. The objective of this annular magnetic baffle was to force the electrons (magnetically) to spiral around the annulus and enter the main discharge chamber in a more uniform (azimuthally) distribution around the annulus. Figure 24 shows a measurement of the current injected into the discharge as a function of the magnetic baffle coil current, J_{MB} (as measured with the probe shown in Figure 22). It is apparent that the annular magnetic baffle is quite effective in producing azimuthal uniformity.

While the electron injection plenum described above achieved the balance in emission and spatial uniformity desired, its use in the multipole discharge chamber resulted in unexpectedly high ion production cost. In fact, more ion current was collected on the walls of the toroidal electron injection plenum enclosure than was extracted in the ion beam. Consequently, if this concept is to become practical, a means must be found for eliminating the ion loss to the plenum walls. Because of the improvement in ion

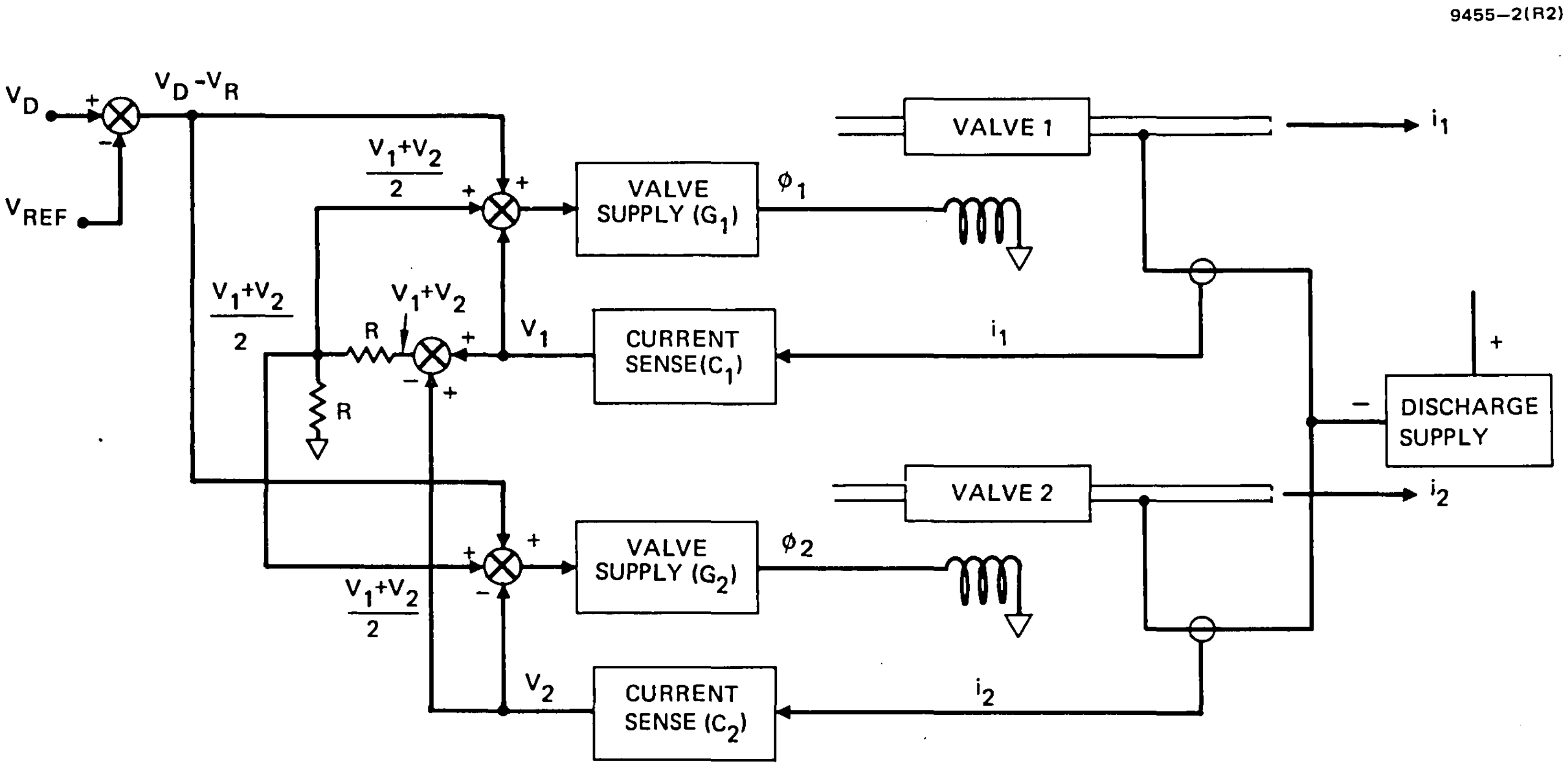

Figure 23. Schematic diagram for emission control balance.

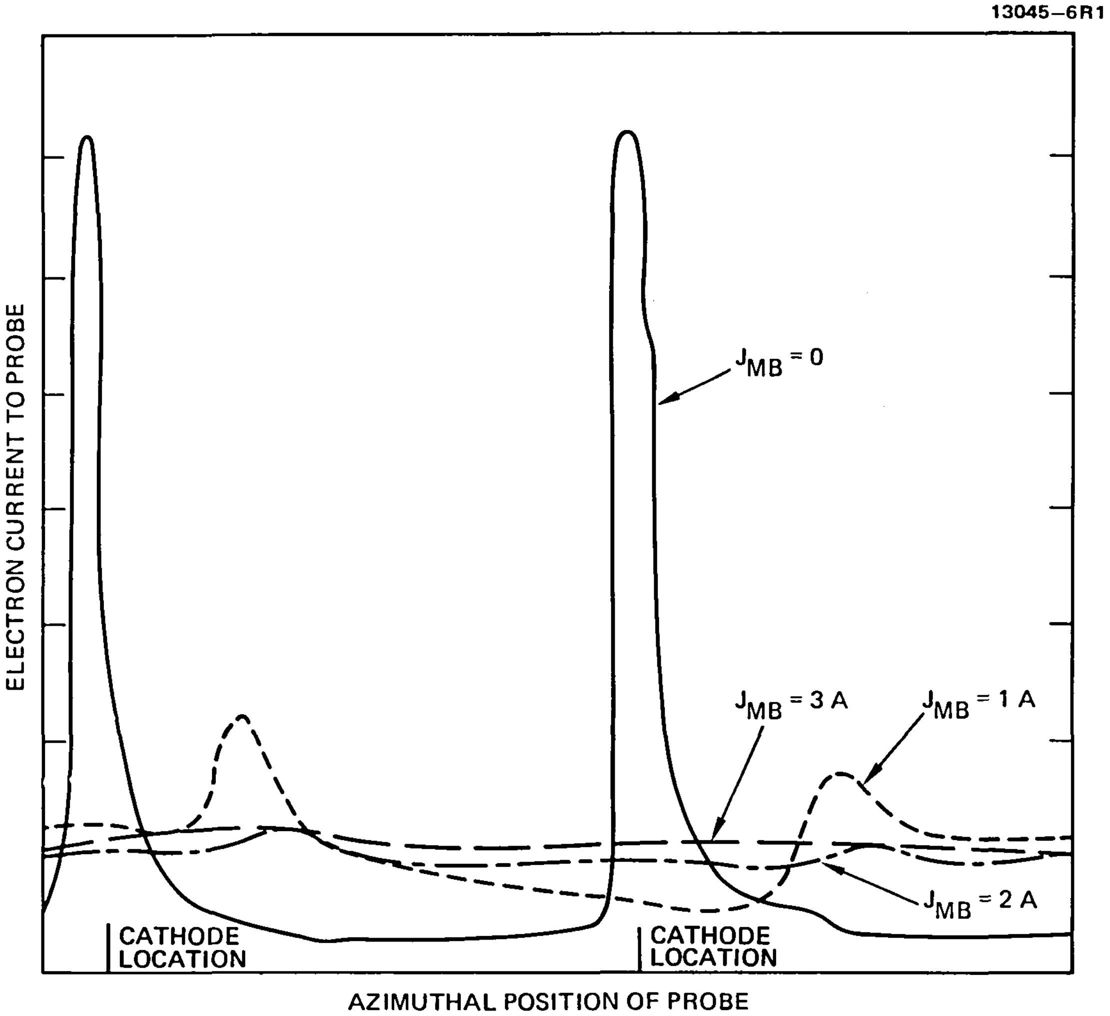

Figure 24. Probe measurement of electron current injected into diode discharge.

production efficiency seen in the ring-cusp discharge chamber, there does not appear to be an immediate requirement to pursue multiple cathode operation.

B. ION EXTRACTION ASSEMBLY TECHNOLOGY

For an inert-gas thruster to produce 0.5 N of thrust at low specific impulse, the ion extraction assembly must focus and accelerate relatively high current densities with relatively low net acceleration voltages. As illustrated in Figure 25 (xenon propellant), this requirement can be met only by using a 3-grid ion extraction assembly. By using a 3-grid assembly, the location of the neutralization surface is fixed (in space) and the ion-optics or focusing properties of the acceleration assembly can be maintained over a wider range of R (the net-total accelerating voltage ratio) than can be maintained with a 2-grid assembly. To achieve the kind of performance indicated in Figure 25, the interelectrode spacing must be maintained with close tolerance at dimensions on the order of 0.5 mm. This close dimensional tolerance dictates a structurally stable electrode and electrode mounting configuration. Excellent results have been obtained by forming the extraction grids with spherically shaped surfaces, so that any deformation that is produced by increased temperature or temperature gradients is controlled (shape remains spherical). The principal challenges remaining are in achieving better control of fabrication processes and in providing a stable support for the electrodes. Progress was made in both areas under this program.

The "standard" 30-cm-diameter, 2-grid mounting structure is shown in Figure 26(a). In the preceding program, it was shown by finite element analysis that the mounting structure must be "soft" in the radial direction to prevent distortion of the grid surface under thermally induced stress. Provision for this flexure requirement was provided in mounting the screen grid on the standard mounting shown as Figure 26(b), but the accel mount was relatively

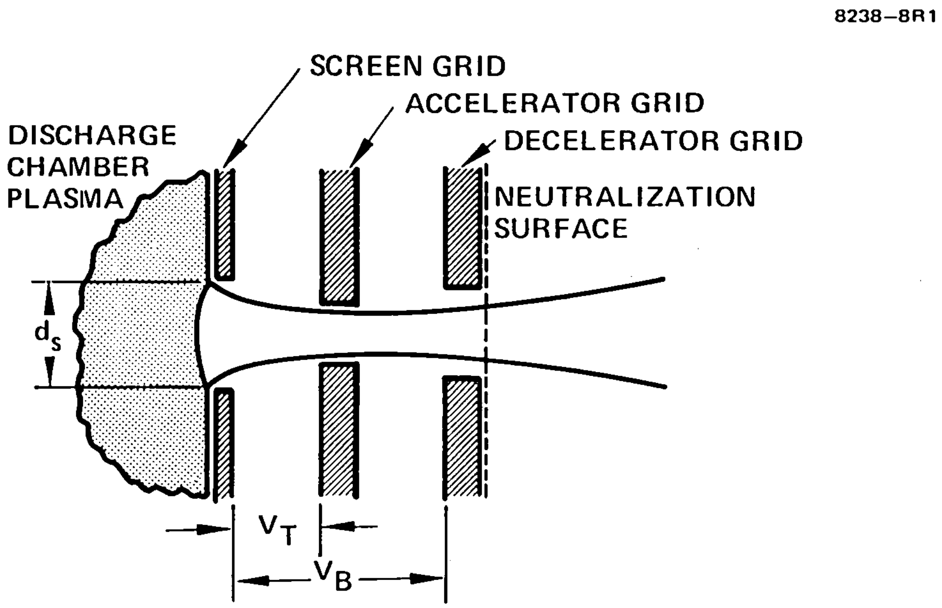

a) THREE-GRID ACCELERATOR SYSTEM

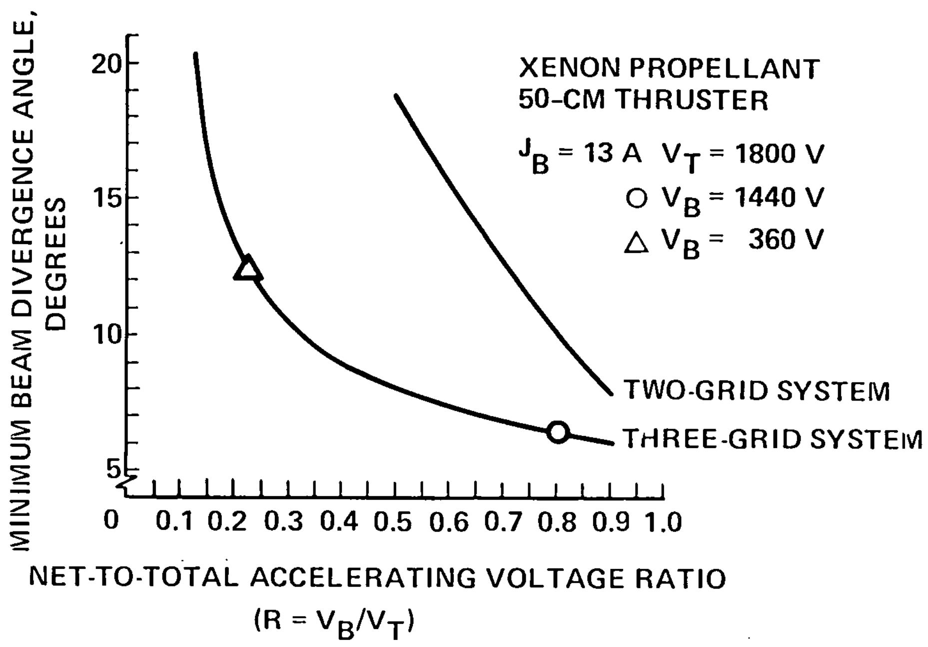

b) BEAM DIVERGENCE AS A FUNCTION OF R

Figure 25. Comparison of 2-grid and 3-grid ion extraction assembly charcteristics.

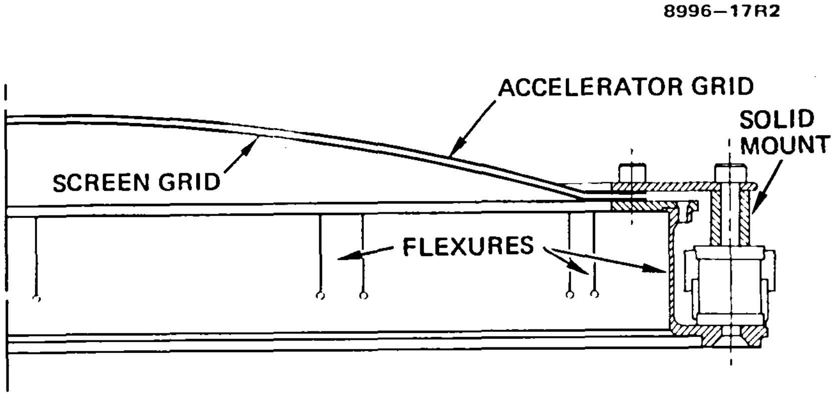

a. J-SERIES DESIGN ("STANDARD")

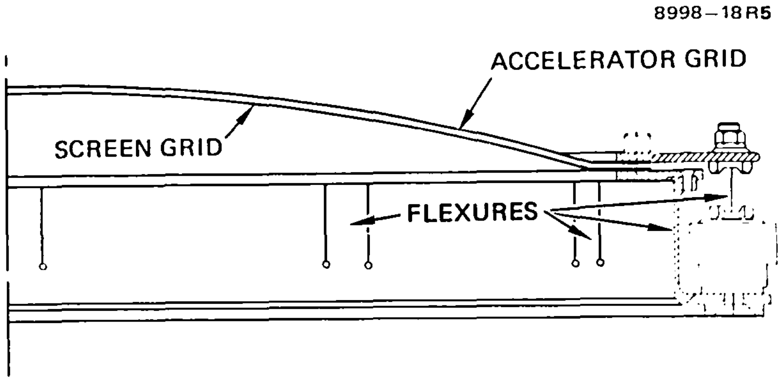

b. ADVANCED TECHNOLOGY 2-GRID DESIGN

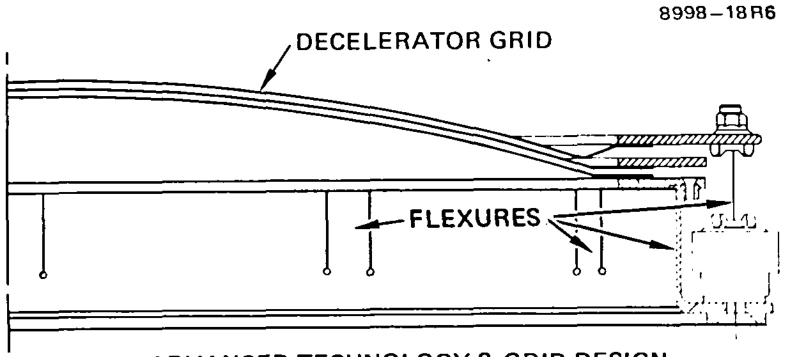

c. ADVANCED TECHNOLOGY 3-GRID DESIGN

Figure 26. Cross sections of the state-of-the-art and advanced-technology ion-optics assemblies.

"stiff." Figure 26(b) shows the accel grid mounting flexure adopted under this program. Incorporation of this feature permitted an increase in the radius of curvature without impairing the ability of the grid to resist distortion. Increasing the radius of curvature is required in order to increase the ion beam diameter to 50 cm without loss of the ability to vector the edge beamlets for producing paraxial beamlet trajectories. Figure 26(c) shows the 3-grid ion extraction assembly mounting that was demonstrated to be successful when tested initially using a mercury ion thruster for both the standard (30 cm) and increased (125 cm) radius of curvature grids.

Fabrication of the grids with longer radius of curvature uncovered shortcomings in the fabrication process that had been causing minor, but detectable distortion in grids with the standard radius of curvature. To describe this deficiency in fabrication procedure, it is necessary to review the procedure for hydroforming spherically shaped or "dished" grids.

In forming dished grids, a fixture is used to clamp the edges of the molybdenum sheets, as shown in Figure 27(a), and hydraulic fluid is forced into the shaded volume to form the grid in a spherical shape. When the hydraulic pressure is removed, the grid relaxes into the shape shown in Figure 27(b) (exaggerated deformation). The "spring back" is caused primarily by the "corner" between the clamped and spherical surface. To restore the spherical surface, the grids must be clamped in a spherical shaped fixture and stress annealed to provide the correct curvature near the corner. The fixture in use was configured, as shown in Figure 28(a), and constructed of "carpenter" steel, which is configurationally stable at the temperatures required for annealing molybdenum. With the molybdenum grids tightly clamped in the annealing fixture, the difference in thermal expansion between carpenter steel and molybdenum at annealing temperature causes the grids to be stretched and further deformed. When the grids and fixture cool, the molybdenum

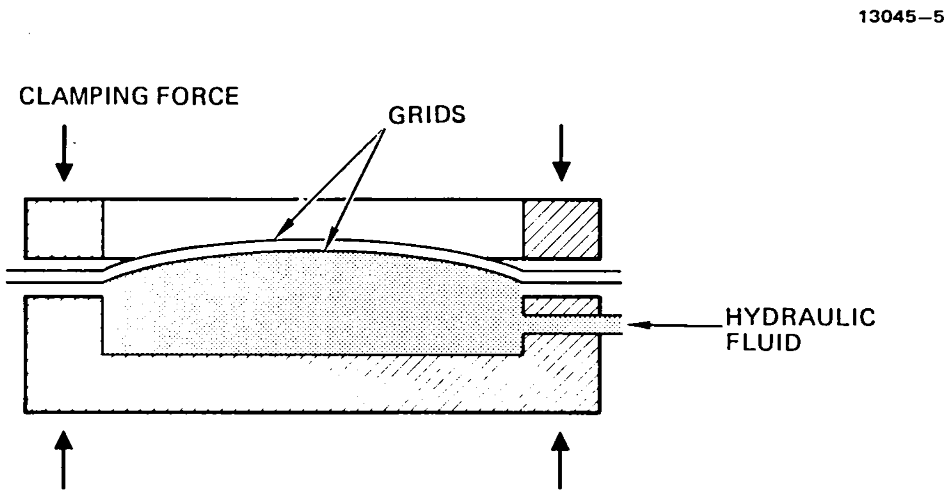

a) HYDROFORMING ION EXTRACTION GRIDS TO OBTAIN SPHERICAL SHAPED SURFACE

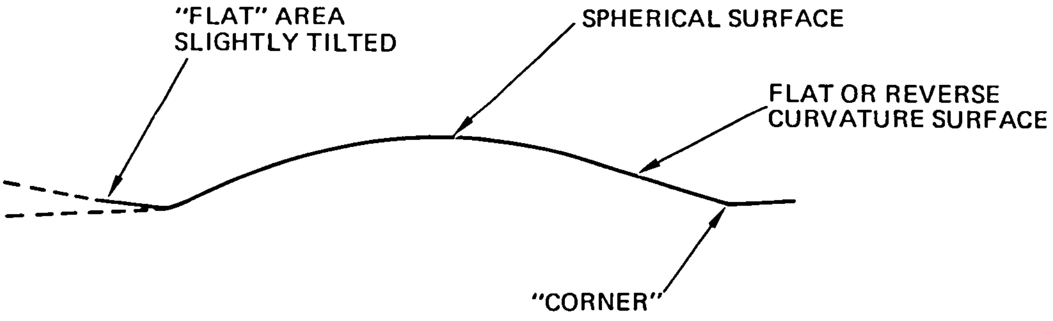

b) GRID SHAPE AFTER HYDROFORMING SHOWING "SPRING-BACK" DISTORTION PRODUCED BY THE "CORNER" MOMENT. STRESS ANNEALING RELAXES MOMENT STRESS AND RESTORES SPHERICAL SURFACE NEAR THE CORNER

Figure 27. Illustration of grid forming procedures and distortion of spherical surface before stress annealing.

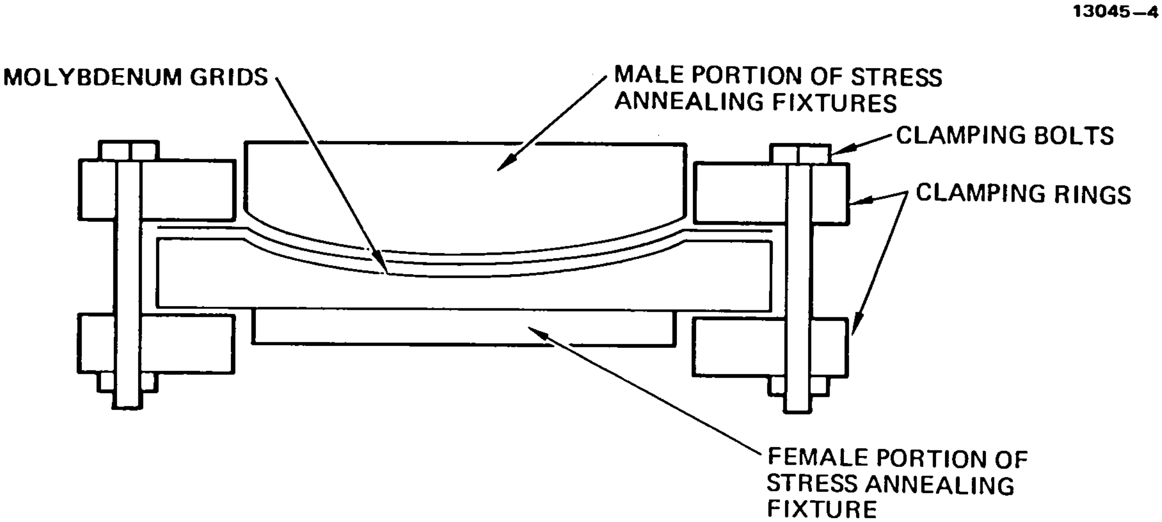

ALL STRESS ANNEALING FIXTURE PARTS CONSTRUCTED OF CARPENTER STEEL

a) STANDARD STRESS ANNEALING FIXTURE USED FOR ALL GRID FABRICATION PRIOR TO THIS PROGRAM

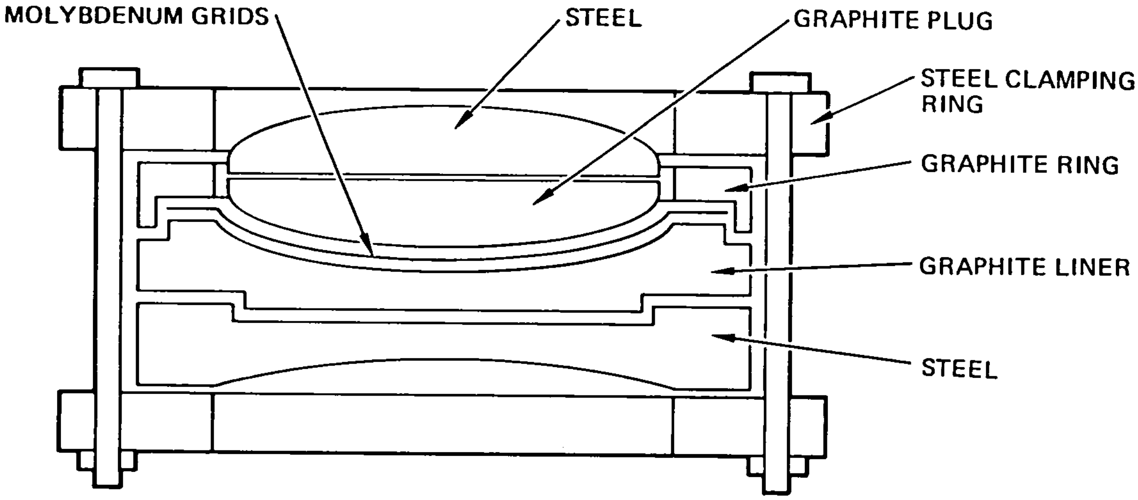

b) STRESS ANNEALING FIXTURE MODIFIED TO PROVIDE GRAPHITE INTERFACE WITH MOLYBDENUM

Figure 28. Standard and modified stress annealing configurations.

experiences radially compressive forces that either distort the aperture pattern or the spherical surface (causes wrinkles). This situation was corrected under this program by fabricating graphite inserts for the stress relieving fixture (shown in Figure 28(b)). While only one grid set was stress annealed in this manner, the results show great promise, and the anomalous successful/unsuccessful results obtained by stress-annealing are considered resolved.

In the process used to form the "stepped" corner of the decel grid (Figure 26(c)), another potential for grid distortion is introduced. The first step of the decel fabrication calls for the formation of a "pie-pan" shaped electrode, as shown in Figure 29(a). The grids are then assembled in the forming fixture, as shown in Figure 29(b), with an air-filled gap as shown. The grid formation proceeds as shown in Figure 29(c) and 29(d), with the trapped air compressed into the annular volume as indicated. When pressure on the hydraulic fluid is released, this compressed air aids the "spring-back" force of the corner and increases the spring-back deformation of the screen and accel grids at their weakest points. We speculate that stress annealing does not completely remove the flat spots, or bumps, noted on the unannealed grids and thermal stress during operation restores these deformations. Failure of the 3-grid ion extraction assemblies used in the LeRC tests is attributed to this type of deformation. The solution to this problem is to eliminate the air gap shown in Figure 29(b) by increasing the depth of the "pie pan" formed in the decel. The subsequent assembly of grids for hydroforming would appear as shown in Figure 30. Notable features of the revised fixture are a deeper pie-pan shape in the decel grid to eliminate the trapped air between the decel and accel grids and locking indents that are pressed into the outer edges of the grids to obtain positive clamping and preventy slipping of the grids during hydroforming. The indentations are located on grid areas that are removed by the chemical milling process. This procedure will be evaluated in future grid fabrication.

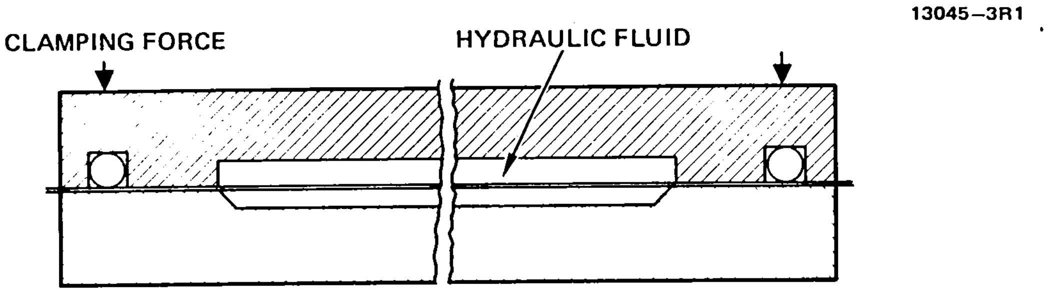

a) FIXTURE FOR FORMING DECEL GRID INTO "PIE-PAN" SHAPE

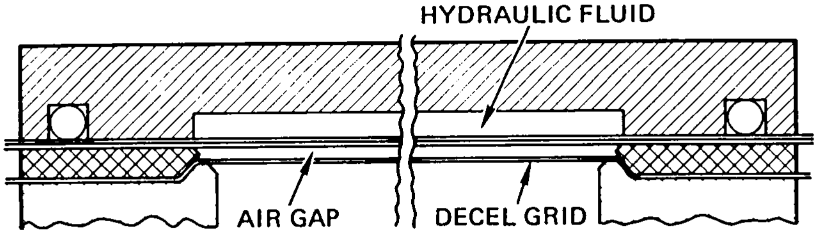

b) GRIDS LOCATED IN FIXTURE FOR HYDROFORMING 3-GRID SET

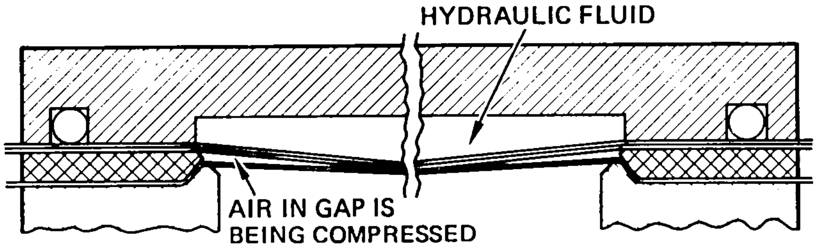

c) GRIDS IN INTERMEDIATE STAGE OF HYDROFORMING, AIR GAP IS BEING COMPRESSED

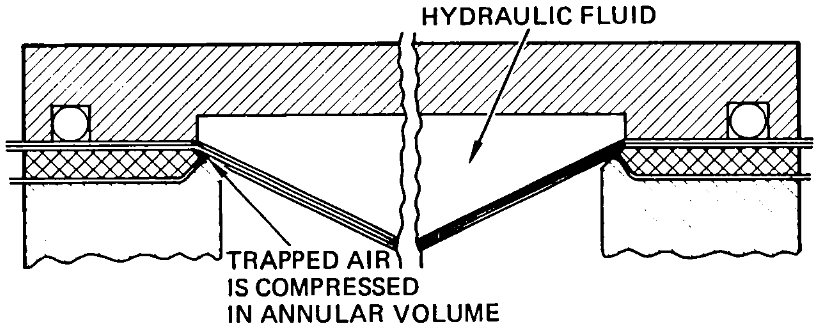

d) GRIDS IN FINAL STAGE OF HYDROFORMING
(BEFORE RELEASE OF HYDRAULIC PRESSURE)

Figure 29. Illustration of hydroforming procedure for 3-grid ion extraction assembly showing compression of gas trapped between accel and decel grids (drawing not to scale).

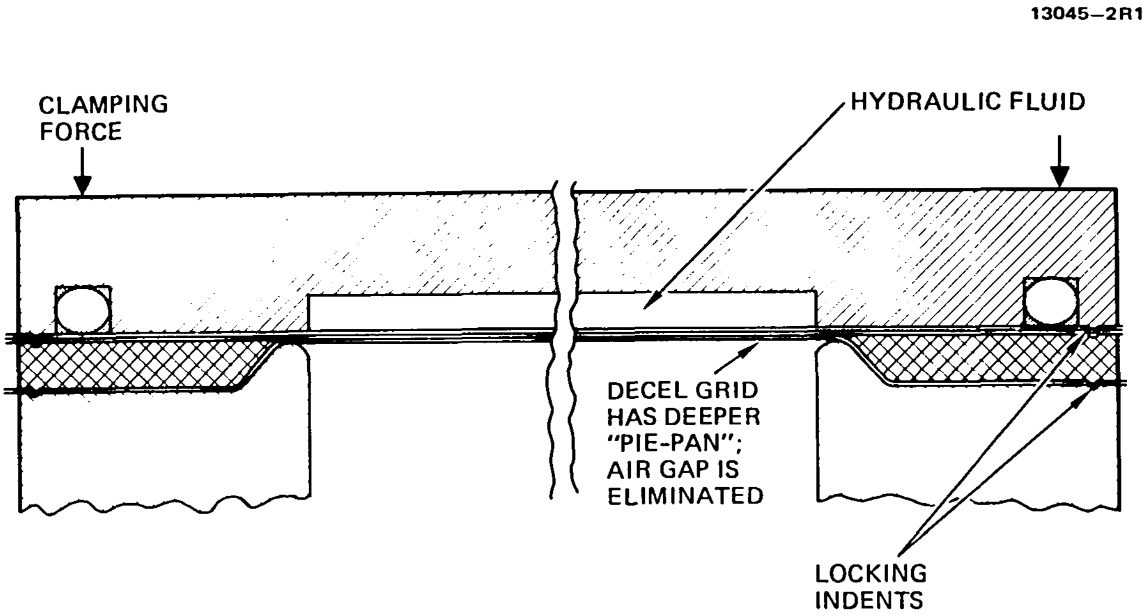

Figure 30. Recommended hydroforming fixture revisions for forming 3-grid electrode set.

C. NEUTRALIZER PERFORMANCE CHARACTERISTICS

As thruster discharge chamber efficiency is increased to achieve ion production costs of less than 100 W/A, the neutralizer power consumption becomes an appreciable performance penalty. This power is lost in the keeper discharge and in coupling the neutralizer emission to the ion beam.

The neutralizer used in this program was configured to be essentially the same as the neutralizer used on the NASA/Hughes 30-cm J-series mercury ion thruster (see Figure 31). The housing and mounting of the gas thruster neutralizer was simplified for ease in assembly and disassembly of the thruster. This neutralizer cathode was operated on argon gas without difficulty in either starting or running. Coupling of electrons from the neutralizer cathode was also readily accomplished with the neutralizer cathode orifice located about 6 cm downstream of and 6-8 cm radially outward from the outermost holes of the accelerator grid. The keeper voltage and voltage to ground (coupling

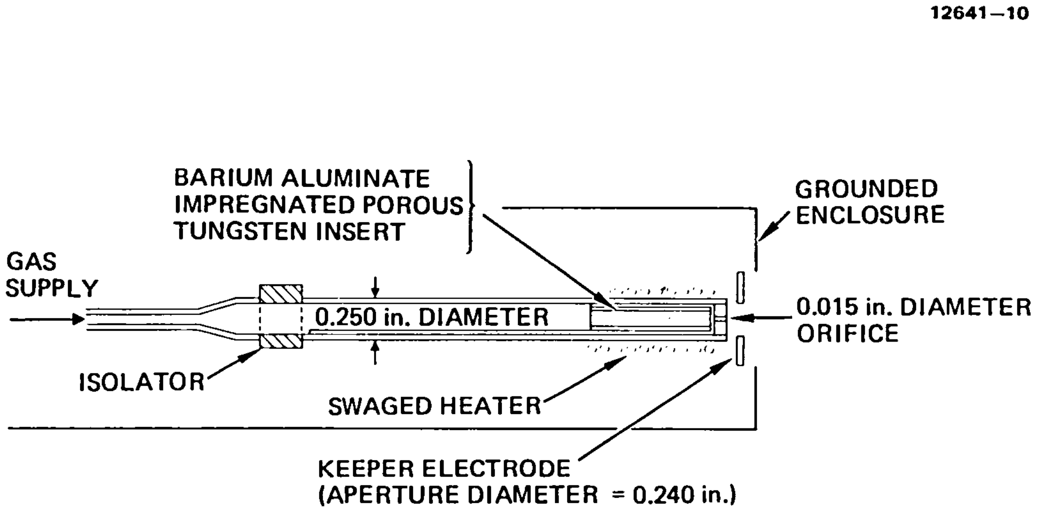

Figure 31. Neutralizer hollow cathode and subassembly components used for inert-gas thruster sets.

voltage) was measured as a function of gas flow with the thruster operating at a 6 A beam current to generate the characteristics shown in Figure 32. These characteristics show that the coupling voltage may be kept in the 20-30 V range even when the keeper current is reduced to 0.5 A, and the flow rate is reduced to about 0.7 A to 0.8 A (equivalent).

The neutralizer performance described here is considered to be representative of the state of the art, though not necessarily the best achievable. The gas flow requirement corresponds to about one gas atom for each 15 electrons, whereas the thruster cathode can be operated with one gas atom for each 20 to 30 electrons. This lower value of neutral atom to electron ratio obtained with the neutralizer cathode results in a reduction of about 10 percent in the overall propellant utilization efficiency of a gas thruster. Operation of the neutralizer cathode at lower gas flow rates results in an increase in the coupling voltage (V_g) and thereby increases the power loss of the thruster by one watt/ampere for each one volt rise in coupling voltage. At 30 W/A, this power loss is comparable to the discharge power loss if ε_I is reduced below 100 W/A.

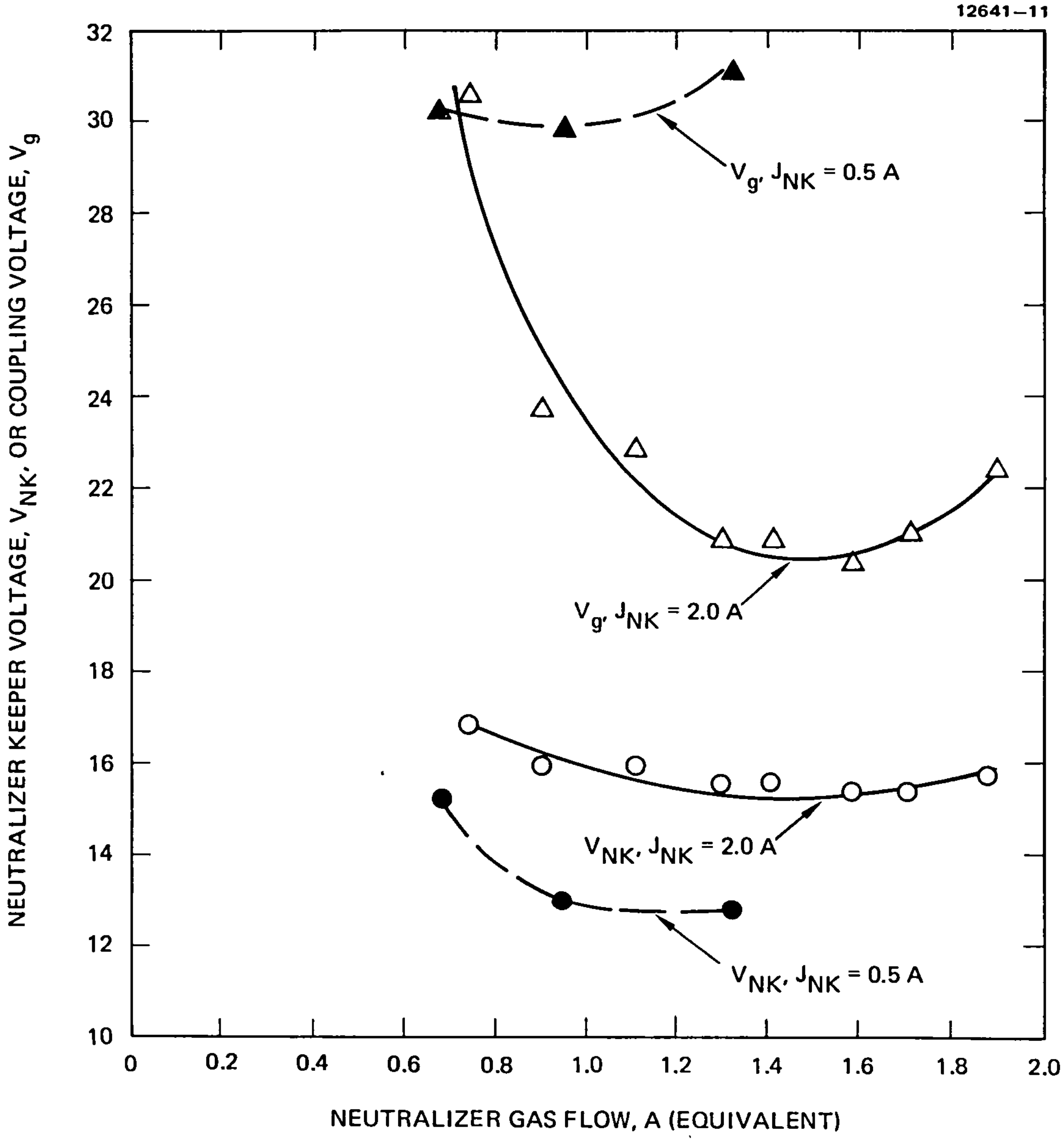

Figure 32. Neutralizer keeper voltage and coupling voltage as functions of gas flow supplied to the neutralizer hollow cathode.

D. QUASI-STEADY-STATE PULSED OPERATION OF INERT GAS THRUSTERS

Having recognized the critical importance of ion-beam extraction in obtaining valid ring-cusp discharge-plasma properties, the capability was established for operating a 30-cm ring-cusp thruster in a pulsed or "quasi-steady-state" mode. In this mode of operation, the discharge is maintained in steady-state operation, and ion-beam extraction is pulsed on for a period of time up to 1 second in duration. Discharge stabilization occurs early during this 1-sec period, and we were able to record reproducible Langmuir probe and wall-probe characteristics during the later portion of the pulse. A typical oscilloscope trace showing several thruster operating parameters during pulsed operation is shown in Figure 33. An important feature of these curves is the stabilization that occurs early in time. This equilibration lends credence to the assertion that quasi-steady-state operation closely resembles continuous thruster operation.

The pulsed-mode operation of the thruster is achieved by programming the gas valves and extraction voltages, as shown in Figure 34. Initial values for the gas-valve settings are determined by steady state operation of the valve and measuring the gas flow with the flow meter. For the main-flow control valve, the voltage is pre-set to provide about 30 to 40 SCCM (indicated). For the cathode-flow gas valve, the start level is set at about 75 SCCM, the run level is set at 8 SCCM, and the idle level is set at 4 SCCM. Figure 35 shows several oscilloscope waveforms of currents and voltages under conditions for which the Langmuir probe characteristic was satisfactorily repeatable. Note that the waveforms for discharge current, J_D, discharge voltage, V_D, and beam current, J_B, have constant values during the time period over which the Langmuir probe characteristic is obtained. The probe voltage, V_p, is with reference to the thruster cathode.

12641-9R1

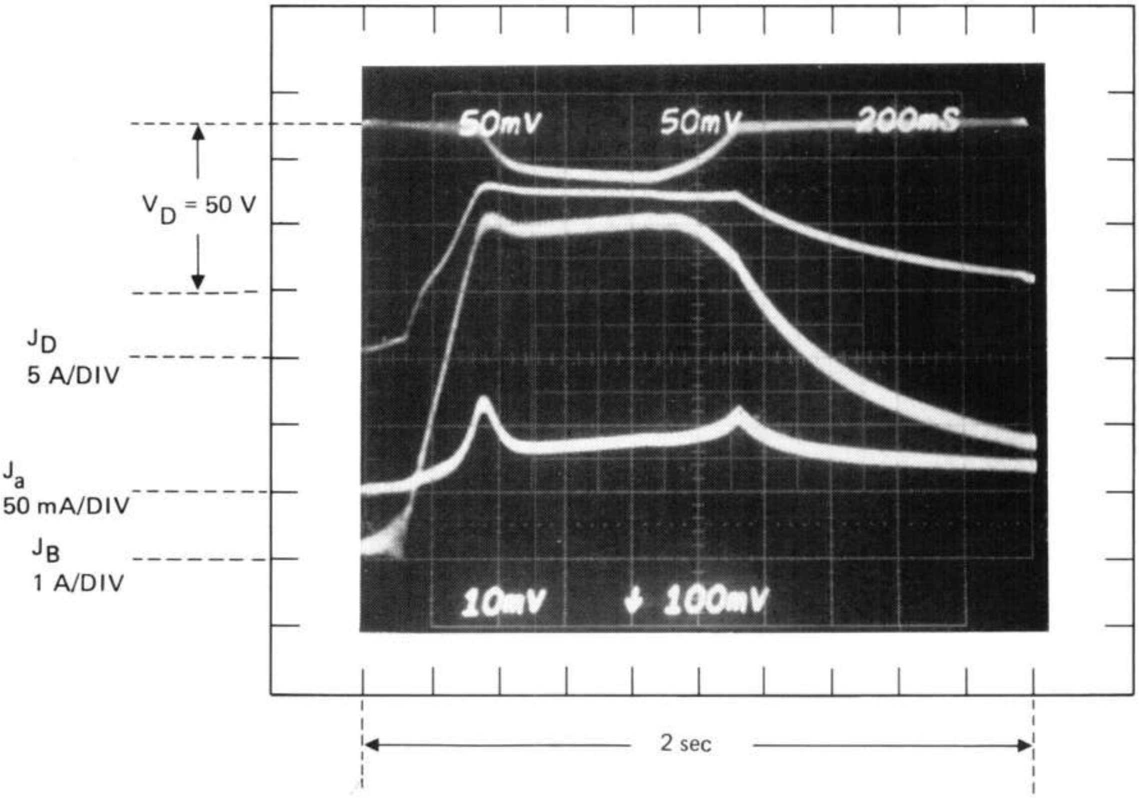

Figure 33. Oscilloscope recording of discharge voltage, V_D, emission current, J_D, accel current, J_a, and beam current, J_B, for pulsed operation of the 30-cm, ring-cusp thruster.

The results of the probe measurements and pulse-mode operation of the ring-cusp thruster were discussed in some detail earlier in the report (section 2). As previously mentioned, the utility of pulse-mode testing as a means of evaluating steady-state performance and plasma properties was not verified satisfactorily. In pulsed mode, the beam current and discharge power tend to be in relatively good agreement with continuous-mode operation, but the discharge impedance (V_D/J_D) and distribution of current to internal electrodes do not correlate well. On the other hand, the plasma

12641-41R1

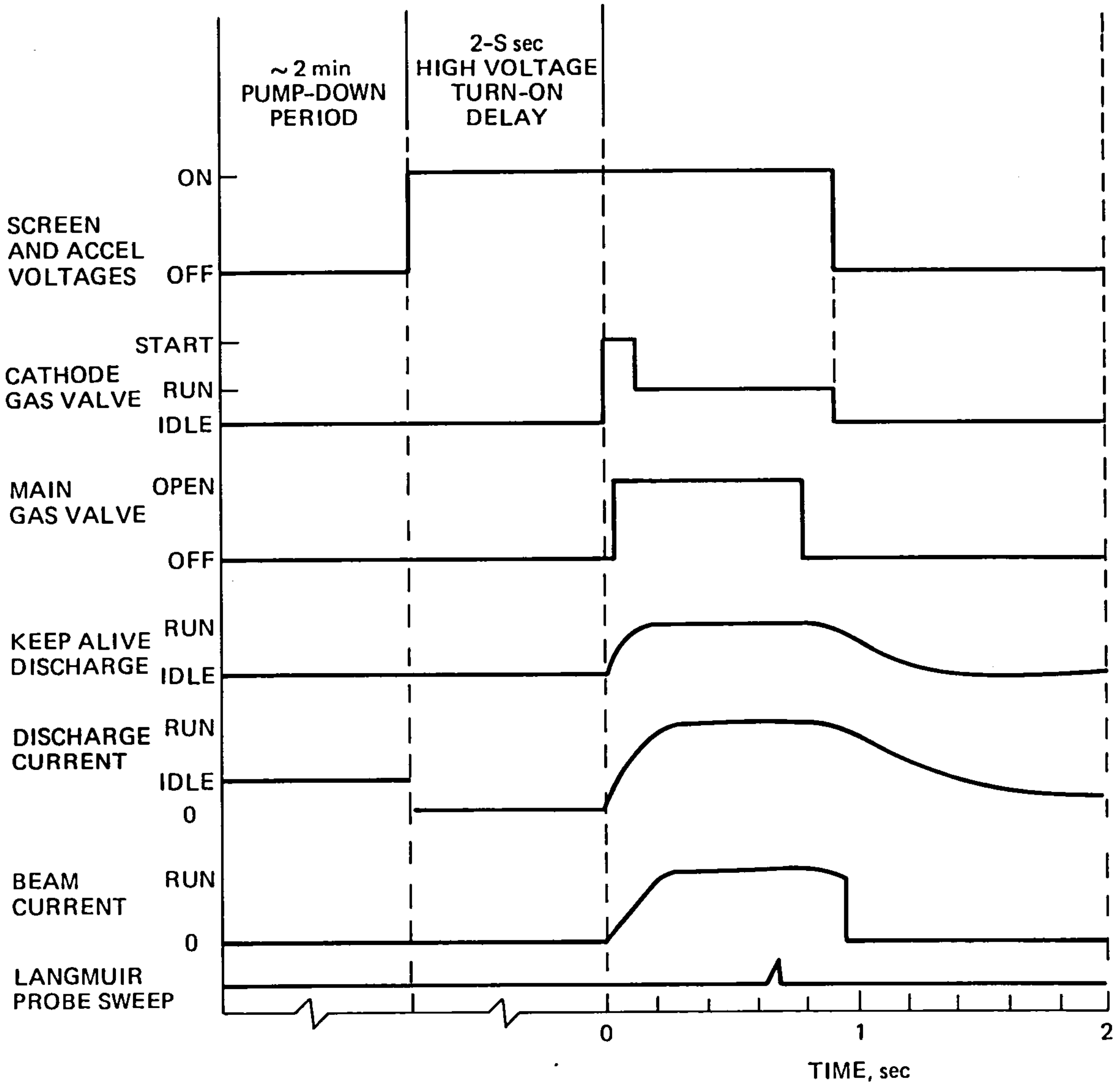

Figure 34. Sequence of valve and power supply control for quasi-steady state, pulsed operation of the ring-cusp thruster as modified for electronically controlled single-shot operation and synchronization of Langmuir probe sweep.

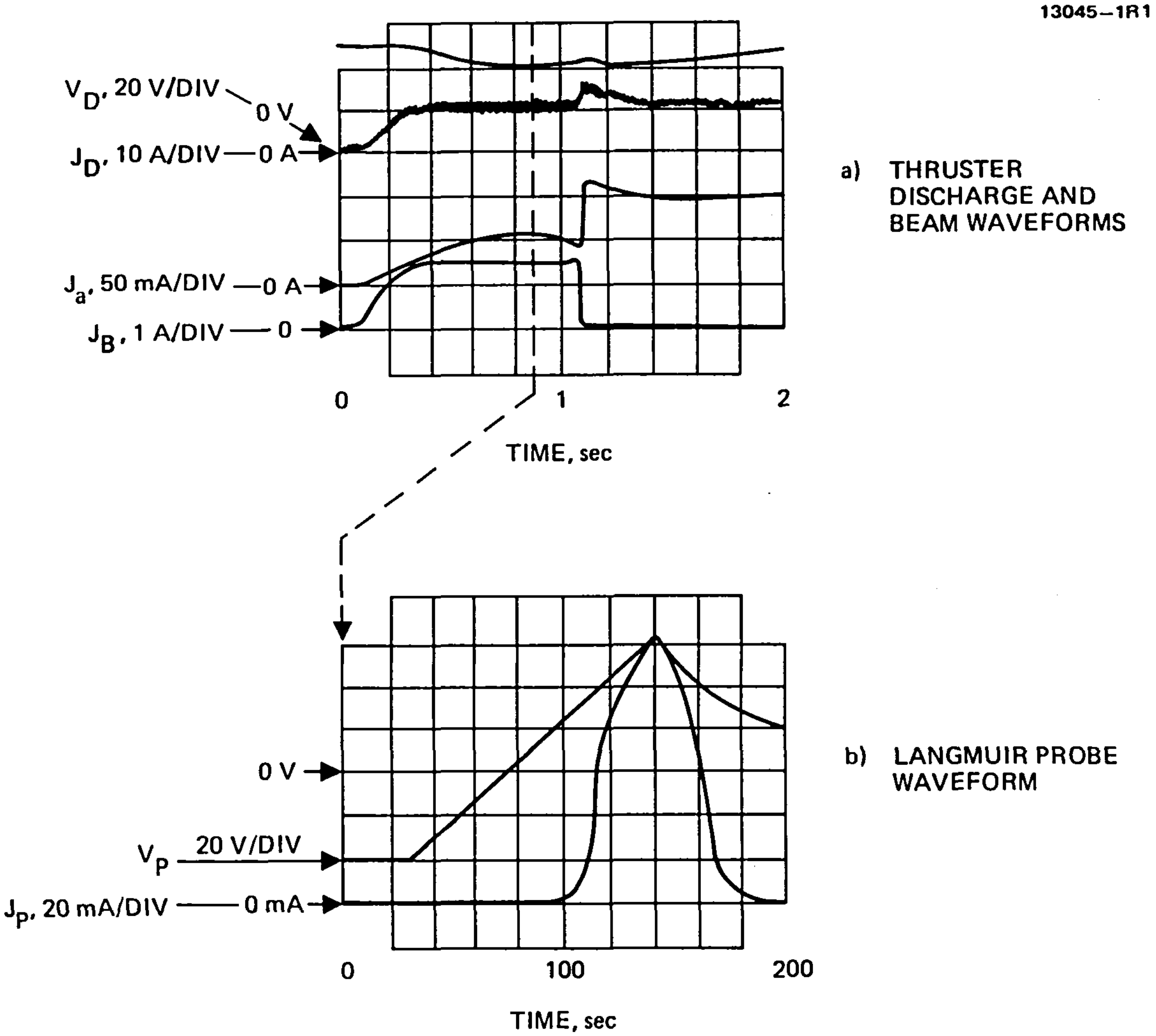

Figure 35. Tracings of oscilloscope waveforms.

properties measured (near the center of the discharge) under pulsed mode are in relatively good agreement with continuous-mode plasma measurements and are more representative than properties measured under beam-off conditions (already discussed in section 2). We attribute the discrepancies in beam current and discharge power to non-equilibrium (thermally dependent) conditions in the hollow cathode, the magnetic circuit and the ion-extraction assembly. If required, these condition could be investigated more completely and pulse-mode operation could probably be improved to better represent continuous mode. The improvements required relate to better control of gas flow (piezoelectric valve drift), and better control of the thermal environment. If testing of a 0.5 N inert-gas thruster at low specific impulse becomes necessary, pulse-mode testing may offer the most cost-effective means for performing these tests.

SECTION 4

CONCLUSIONS

The investigation of inert-gas electrostatic ion thrusters under this program produced a new and expanded understanding of ion thruster discharge chamber processes. Previously, theory predicted, and experimental results seemed to confirm, that ions were lost from the discharge plasma isotropically. Under this premise the ratio of the plasma volume area to extraction grid area unequivocally defines the ion production cost and subsequently sets limits on electrical efficiency. Measurements performed on a ring-cusp discharge chamber conflict with this premise and the assumption of isotropic ion losses was found to be inappropriate. A strong dependence of discharge chamber operation on the ion extraction assembly was observed, and the data indicate the presence of a directed ion drift. We attribute this observation to the extremely high magnetic field strength of the magnetic cusps in the ring-cusp thruster and a gradient in field strength in the direction of the extraction screen. This magnetic field configuration controls electron loss very effectively and thereby eliminates the requirements for ion flux at Bohm velocity, except at the extraction-screen/plasma boundary. The net result is that ion production costs that approach the plasma volume cost (50 W/A) may be achievable with ring-cusp magnetic geometries. Under this program, 100 W/A were achieved more or less routinely with good propellant efficiencies using both argon and xenon propellants.

The ion extraction assembly remains the most critical assembly of the ion thruster from both a performance and fabrication standpoint. Under this program, thermomechanical stability of the extraction grids was demonstrated with two, 3-grid ion extraction assembly designs, one with the 1.25 m radius of curvature that is required for 50-cm thruster grids. Two fabrication procedures were identified that may result in built-in stresses that lead to deformation during operation. One of these procedural difficulties was corrected under the program; the other will be corrected in future grid fabrication.

REFERENCES

1. G.C. Isaacson, "Multipole Gas Thruster Design," NASA CR-135110, for Grant NSG-3011, June 1977.

2. H.R. Kaufman and P.J. Wilbur, "Scaling of Mercury and Gaseous Propellant Ion Thrusters to Large Sizes," AIAA 78-667. Presented at AIAA 13th International Electric Propellant Conference, San Diego, California, April 1978.

3. J.S. Sovey, "Performance of Magnetic Multipole Line-Cusp Argon Ion Thruster,"J. Spacecraft and Rockets, 19, No. 3, 257-262 (May-June 1982).

4. J.S. Sovey, "Improved Ion Containment Using a Ring-Cusp Ion Thruster," AIAA Paper 82-1928, November 1982.

5. R.D. Moore, "Magneto-Electrostatically Contained Plasma Ion Thruster," AIAA Paper 69-260, March 1969.

6. H.R. Kaufman, R.S. Robinson, and L.E. Frisa, "Ion-Flow Experiments in a Multipole Discharge Chamber," AIAA Paper 82-1930, November 1982.

7. J.R. Brophy and P.J. Wilbur, "The Flexible Magnetic Field Thruster," AIAA Paper 82-1936, November 1982.

8. E.H. Holt and R.E. Haskell, Plasma Dynamics (Macmillan Co., New York, 1965).

9. D. Bohm, "Minimum Ion Kinetic Energy for a Stable Sheath," Characteristics of Electrical Discharges in Magnetic Fields, A. Gutherie and R.K. Wakerling, Editors (McGraw-Hill Book Co., New York, 1949), pp. 77-86.

DISTRIBUTION LIST

	Copies
National Aeronautics and Space Administration	
Washington, DC 20546	
Attn: MP-3/Mr. Ivan Bekey	1
RTS-6/Mr. Wayne Hudson	1
RTS-6/Mr. Jerome Mullin	1
RSE-5/Mr. David Byers	1
National Aeronautics and Space Administration	
Lewis Research Center	
21000 Brookpark Road	
Cleveland, OH 44135	
Attn: Space Technology Section, MS 500-305	1
Technology Utilization Office, MS 3-19	1
Report Control Office, MS 5-5	1
Library, MS 60-3	2
Mr. N. Musial, MS 500-113	1
Dr. M. Goldstein, Chief Scientist, MS 5-3	1
Mr. T. Cochran, MS 501-7	1
Mr. F. Terden, MS 501-7	1
Mr. V. Rawlin, MS 501-7	1
Mr. J. Sovey, MS 501-7	90
National Aeronautics and Space Administration	
Marshall Space Flight Center	
Huntsville, AL 35912	
Attn: Mr. Robert Bechtel	1
Research and Technology Division	
Wright-Patterson AFB, OH 45433	
Attn: (ADTN) Mr. Everett Bailey	1
NASA Scientific and Technical	
Information Facility	
P.O. Box 8757	
Baltimore, MD 21240	
Attn: Accessioning Dept.	6
DST 1	
Ministry of Defence	
Metropole Building	
Northumberland Avenue	
London, WC2 N5BL England	
Attn: Dr. D.G. Fearn	1
National Aeronautics and Space Administration	
Goddard Space Flight Center	
Greenbelt, MD 20771	
Attn: Dr. David H. Suddreth	1

	Copies
COMSAT Laboratories	
P.O. Box 115	
Clarksburg, MD 20734	
Attn: Mr. B. Free	1
Intelsat	
490 L'Enfant Plaza, S.W.	
Washington, DC 20024	
Attn: Mr. Rolland Schreib	1
Rocket Propulsion Laboratory	
Edwards AFB, CA 93523	
Attn: LKDH/Mr. Frank Meade	2
LKDH/Capt. Elledge	1
Giessen University	
1st Institute of Physics	
Giessen, West Germany	
Attn: Professor H.W. Loeb	1
Jet Propulsion Laboratory	
4800 Oak Grove Drive	
Pasadena, California 91102	
Attn: Technical Library	1
Dr. K. Atkins	1
Dr. R. Vondra	1
Mr. Dennis Fitzgerald	1
Dr. Graeme Aston	1
Electro-Optical Systems, Inc.	
300 North Halstead	
Pasadena, California 91107	
Attn: Mr. E. James	1
Mr. W. Ramsey	1
TRW Inc.	
TRW Systems	
One Space Park	
Redondo Beach, California 90278	
Attn: Mr. Sid Zafran	1
National Aeronautics and Space Administration	
Ames Research center	
Moffett Field, California 94035	
Attn: Technical Library	1
National Aeronautics and Space Administration	
Langley Research Center	
Langley Field Station	
Hampton, Virginia 23365	
Attn: Technical Library	1

	Copies
Hughes Research Laboratories	
3011 Malibu Canyon Road	
Malibu, California 90265	
Attn: Mr. J.H. Molitor	1
Dr. R.L. Poeschel	1
Dr. Jay Hyman	1
Dr. J.R. Beattie	1
Dr. W.S. Williamson	1
Dr. H.J. King	1
Princeton University	
Princeton, NJ 08540	
Attn: Dean R.G. Jahn	1
Dr. Arnold Kelly	1
Boeing Aerospace Co.	
P.O. Box 3999	
Seattle, Washington 98124	
Attn: Mr. Donald Grim, MS 8K31	1
Electrotechnical Laboratory	
1-1-4, Umezono, Sakura-Mura,	
Niihari-Gun	
Ibaraki, Japan	
Attn: Dr. Katsuya Nakayama	1
Michigan State University	
East Lansing, MI 48824	
Attn: Dr. J. Asmussen	1
Dr. M.C. Hawley	1
The Aerospace Corporation	
Space SCiences Lab.	
P.O. Box 92957	
Los Angeles, California 90009	
Attn: Mr. T. Silva	1
Department of Aeronautics	
Faculty of engineering	
Universilty of Tokyo	
7-3-1, Hongo, Bunkyo-Ku	
Tokyo, Japan	
Attn: Prof. Itsuro Kimura	1
Dr. Pradosh Ray	
Tuskegee Institute	
School of Engineering	
Tuskegee Institute, AL 36088	1

Copies

Dr. Chris Olson
Dept. of Physics
University of Huntsville
Huntsville, AL 35899 1

Dr. Kevin Rudolph
MS. M0482
Martin Marietta Aerospace
P.O. Box 179
Denver, CO 80201 1

Dr. Rolf Bühler
Institut Für Raumfahrtantriebe
Universitat Stuttgart
7 Stuttgart 80
Pfaftenwaldring 31
West Germany 1

Colorado State University
Fort Collins, CO 80523
Attn: Dr. H.R. Kaufman 1
Dr. R.S. Robinson 1
Dr. P.J. Wilbur 1

Dr. David Finkelstein
Dept. of Physics
Georgia Institute of Technology
Atlanta, GA 30332 1